

# A simple derivation of moiré-scale continuous models for twisted bilayer graphene

Éric Cancès<sup>1</sup>, Louis Garrigue<sup>2</sup>, and David Gontier<sup>3</sup>

<sup>1</sup>CERMICS, École des Ponts and Inria Paris, 6 and 8 av. Pascal, 77455 Marne-la-Vallée, France.  
(eric.cances@enpc.fr)

<sup>2</sup>CERMICS, École des Ponts and Inria Paris, 6 and 8 av. Pascal, 77455 Marne-la-Vallée, France.  
(louis.garrigue@enpc.fr)

<sup>3</sup>CEREMADE, University of Paris-Dauphine, PSL University, 75016 Paris, France & ENS/PSL  
University, Département de Mathématiques et Applications, F-75005, Paris, France.  
(gontier@ceremade.dauphine.fr)

June 14, 2022

## Abstract

We provide a formal derivation of a reduced model for twisted bilayer graphene (TBG) from Density Functional Theory. Our derivation is based on a variational approximation of the TBG Kohn-Sham Hamiltonian and asymptotic limit techniques. In contrast with other approaches, it does not require the introduction of an intermediate tight-binding model. The so-obtained model has a mathematical structure similar to that of the Bistritzer-MacDonald (BM) model but it contains some additional terms. Its parameters can be easily computed from Kohn-Sham calculations on single-layer graphene and untwisted bilayer graphene with different stacking. It allows one in particular to estimate the parameters  $w_{AA}$  and  $w_{AB}$  of the BM model from first-principles. The resulting numerical values, namely  $w_{AA} = w_{AB} \simeq 126$  meV for the experimental interlayer mean distance are in good agreement with the empirical values  $w_{AA} = w_{AB} = 110$  meV obtained by fitting to experimental data. We also show that if the BM parameters are set to  $w_{AA} = w_{AB} \simeq 126$  meV, the BM model is an accurate approximation of our reduced model.

## 1 Introduction

Moiré materials [1, 9] have attracted a lot of interest in condensed matter physics since, notably, the experimental discovery of Mott insulating and nonconventional superconducting phases [8] in twisted bilayer graphene (TBG) for specific small twist angles  $\theta$ . In particular, the experiments reported in [8] were done with  $\theta \simeq 1.1^\circ$ . For such small twist angles, the moiré pattern is quite large and typically contains of the order of 11,000 carbon atoms. In addition, the system is aperiodic (incommensurate), except for a countable set of values of  $\theta$ . All this makes brute force first-principle calculations extremely challenging.

Most theoretical investigations on TBG rely on continuous models [22, 5, 6, 26] such as the Bistritzer-MacDonald (BM) model [6], an effective continuous periodic model describing low-energy excitations in TBG close to half-filling. The BM Hamiltonian is a self-adjoint operator on  $L^2(\mathbb{R}^2; \mathbb{C}^4)$  given by

$$H_\theta^{\text{BM}} = \begin{pmatrix} v_F \boldsymbol{\sigma}_{\theta/2} \cdot (-i\nabla) & \mathbf{V}(k_\theta \mathbf{x}) \\ \mathbf{V}(k_\theta \mathbf{x})^* & v_F \boldsymbol{\sigma}_{-\theta/2} \cdot (-i\nabla) \end{pmatrix}, \quad (1)$$

where  $v_F$  is the Fermi velocity in single-layer graphene,  $\sigma_{\pm\theta/2} = e^{\mp i\frac{\theta}{4}\sigma_3}(\sigma_1, \sigma_2)e^{\pm i\frac{\theta}{4}\sigma_3}$ , with

$$\sigma_1 = \begin{pmatrix} 0 & 1 \\ 1 & 0 \end{pmatrix}, \quad \sigma_2 = \begin{pmatrix} 0 & -i \\ i & 0 \end{pmatrix}, \quad \sigma_3 = \begin{pmatrix} 1 & 0 \\ 0 & -1 \end{pmatrix}, \quad (2)$$

and  $k_\theta = \frac{8\pi}{3a_0} \sin(\theta/2)$ , with  $a_0$  the single-layer graphene lattice constant. The function  $\mathbf{V} : \mathbb{R}^2 \rightarrow \mathbb{C}^2$  is quasi-periodic at the so-called moiré scale (see Section 3.4 for details) and depends on two empirical parameters  $w_{AA}$  and  $w_{AB}$  describing interlayer coupling in AA and AB stacking respectively. A rigorous mathematical derivation of the BM model from a tight-binding Hamiltonian whose parameters satisfy suitable scaling laws, was recently proposed in [29]. A simplified chiral BM model, obtained by setting  $w_{AA} = 0$ , was notably used in [27, 2, 30] to prove the existence of perfectly flat bands at the Fermi level for a sequence of so-called “magic” angles. From a physical point of view, the existence of partially occupied almost flat bands in the single-particle picture may reflect the presence of localized strongly correlated electrons, and provide a possible explanation of the experimentally observed superconducting behavior [25]. An alternative approach to using effective models at the moiré scale is to develop atomic-scale models and efficient computational methods adapted to incommensurate 2D heterostructures [20, 18, 13, 11, 21].

This article is concerned with the derivation of BM-like effective models from Density Functional Theory (DFT). We start from an approximation of the TBG Kohn-Sham potential obtained, as proposed in [28], by summing the (translated and rotated) Kohn-Sham potentials of each layer and adding a correction  $V_{\text{int}}$  depending only on the transverse variable  $z$ . We then perform a variational approximation of the resulting Kohn-Sham Hamiltonian in the space of wave packets with an envelope oscillating at the mesoscopic moiré scale, and constructed from the four atomic-scale Bloch functions at the Dirac point  $\mathbf{K}$  of the two (twisted and translated) single layers. Such wave packets are meant to describe low energy excitations in the  $\mathbf{K}$ -valley close to half-filling. In the small twist angle limit and after proper rescaling of the space and time variables, this variational approximation gives rise to a time-dependent BM-like model set on the state space  $L^2(\mathbb{R}^2; \mathbb{C}^4)$ . The effective scalar and vector potentials appearing in this model can be computed from the single-layer graphene Kohn-Sham potential and Bloch waves at point  $\mathbf{K}$ , as well as the correction potential  $V_{\text{int}}$ . The latter is obtained by averaging over all possible stacking a correction potential computed for untwisted bilayer graphene. Let us emphasize that, in contrast with other approaches [6, 23, 10, 15, 19, 3, 29], our derivation does not involve an intermediate tight-binding model and is based on real-space (not momentum-space) computations.

The paper is organized as follows. After reviewing the basic properties of single-layer graphene used in this work, we recall in Section 2 the structure of the approximate Kohn-Sham Hamiltonian for twisted bilayer graphene introduced in [28]. We then define in Section 3.1 its variational approximation in the regime of low-energy excitations in the  $\mathbf{K}$ -valley. By identifying the leading order terms of this approximation in the limit of small twist angles, we derive in Section 3.2 an effective time-dependent BM-like model with scalar and vector potentials that can be computed from first-principles. We study the symmetries of this model in Section 3.3. The connection with the BM model is discussed in Section 3.4. We gather some numerical simulation in Section 4. In particular, we derive first-principle values for the BM parameters  $w_{AA}$  and  $w_{AB}$  for the experimental interlayer mean distance and check that the BM model with these specific parameters is an accurate approximation of our reduced model. Our simulations were performed with the DTFK software [17], a recently developed DFT code in Julia particularly well suited to test new algorithms and numerical methods. The mathematical derivation of the reduced model

is detailed in Appendix A. The technicalities arising from the nonlocal component of the pseudopotential in planewave DFT calculations are postponed until Appendix B.

Our derivation is done on the *unrelaxed* configuration. As explained in Remark 5, it is however possible to take atomic relaxation into account in our reduced model by modifying the effective potentials according to the atomic displacement field. It is also possible to include both the  $\mathbf{K}$  and  $\mathbf{K}'$  valleys in a unified framework, leading to an eight-component effective model. The case of relaxed configurations, the construction of the band diagrams for both unrelaxed and relaxed configurations, and the eight-component model will be dealt with in future works.

## 2 Approximation of the Kohn-Sham Hamiltonian for TBG

### 2.1 Single-layer graphene

We first set up some notation and recall the basic properties of single-layer graphene one-particle band diagram that are relevant for this work. We denote the position variable by  $\mathbf{r} \in \mathbb{R}^3$  and decompose it as  $\mathbf{r} = (\mathbf{x}, z)$  where  $\mathbf{x} = (x_1, x_2) \in \mathbb{R}^2$  and  $z \in \mathbb{R}$  are respectively the longitudinal (in-plane) and transverse (out-of-plane) position variables. We denote by

$$R_\theta := \begin{pmatrix} \cos \theta & -\sin \theta \\ \sin \theta & \cos \theta \end{pmatrix} = \cos \theta \mathbb{I}_2 + \sin \theta J, \quad \text{with} \quad J := \begin{pmatrix} 0 & -1 \\ 1 & 0 \end{pmatrix},$$

the 2D rotation matrix of angle  $\theta \in \mathbb{R}$ . For  $\mathbf{y} \in \mathbb{R}^2$ ,  $\theta \in \mathbb{R}$ , and  $f : \mathbb{R}^3 \rightarrow \mathbb{C}$ , we set

$$\begin{aligned} (\tau_{\mathbf{y}} f)(\mathbf{x}, z) &:= f(\mathbf{x} - \mathbf{y}, z), & (\text{horizontal translation of vector } \mathbf{y}), \\ (\mathcal{R}_\theta f)(\mathbf{x}, z) &:= f(R_{-\theta} \mathbf{x}, z), & (\text{rotation of angle } \theta \text{ around the } z\text{-axis}), \\ (\mathfrak{R} f)(x_1, x_2, z) &:= f(x_1, -x_2, -z) & (\text{rotation of angle } \pi \text{ around the } x_1\text{-axis}), \\ (\mathcal{P} f)(\mathbf{x}, z) &= (\mathcal{R}_\pi f)(\mathbf{x}, z) := f(-\mathbf{x}, z), & (\text{in-plane parity operator}), \\ (\mathcal{C} f)(\mathbf{r}) &:= \overline{f(\mathbf{r})}, & (\text{complex conjugation}), \\ (\mathcal{S} f)(\mathbf{x}, z) &:= f(\mathbf{x}, -z) & (\text{mirror symmetry w.r.t. the plane } z = 0). \end{aligned}$$

By a slight abuse of notation, we will also denote by  $\tau_{\mathbf{y}}$ ,  $\mathcal{R}_\theta$ ,  $\mathfrak{R}$ ,  $\mathcal{P}$ , and  $\mathcal{C}$  the operators acting on functions  $f : \mathbb{R}^2 \rightarrow \mathbb{C}$  of the longitudinal position variables.

We consider in this section a graphene single-layer in the horizontal plane  $z = 0$  with Bravais lattice

$$\mathbb{L} = \mathbb{Z}\mathbf{a}_1 + \mathbb{Z}\mathbf{a}_2 \quad \text{with} \quad \mathbf{a}_1 = a_0 \begin{pmatrix} 1/2 \\ -\sqrt{3}/2 \end{pmatrix} \quad \text{and} \quad \mathbf{a}_2 = a_0 \begin{pmatrix} 1/2 \\ \sqrt{3}/2 \end{pmatrix},$$

where  $a_0 = \sqrt{3}a$  is the graphene lattice constant ( $a \simeq 0.142 \text{ nm} \simeq 2.68 \text{ bohr}$  is the carbon-carbon nearest neighbor distance). Each periodic cell contains two carbon atoms, giving rise to the A and B sublattices  $\mathbb{L} + \frac{2}{3}\mathbf{a}_1 + \frac{1}{3}\mathbf{a}_2$  and  $\mathbb{L} + \frac{1}{3}\mathbf{a}_1 + \frac{2}{3}\mathbf{a}_2$  (see Fig. 1). The space group of graphene is  $\text{Dg80} = \text{D}_{6h} \ltimes \mathbb{L}$  ( $\text{p6/mmm}$ ), where  $\text{D}_{6h}$  is the group of order 24 generated by e.g.  $\mathcal{R}_{\frac{\pi}{3}}$ ,  $\mathfrak{R}$  and  $\mathcal{S}$ . As a consequence, the single-layer graphene Kohn-Sham potential  $V$  is  $\mathbb{L}$ -translation invariant and has the honeycomb symmetry. It is also real-valued. We therefore have

$$\forall \mathbf{R} \in \mathbb{L}, \quad \tau_{\mathbf{R}} V = V, \quad \forall g \in \text{D}_{6h}, \quad gV = V, \quad \mathcal{C}V = V. \quad (3)$$

The single-layer graphene Kohn-Sham Hamiltonian reads

$$H^{(1)} := -\frac{1}{2}\Delta + V. \quad (4)$$

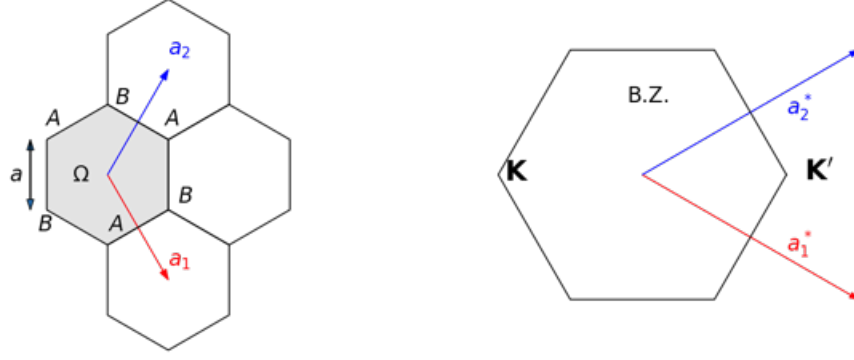


Figure 1: Single-layer graphene. Left: atomic positions of the carbon atoms (A and B sublattices) in the physical space, and lattice vectors  $\mathbf{a}_1$  and  $\mathbf{a}_2$ . Right: reciprocal lattice vectors  $\mathbf{a}_1^*$  and  $\mathbf{a}_2^*$ , and first Brillouin zone in momentum space; the positions of the  $\mathbf{K}$  and  $\mathbf{K}'$  Dirac points are also indicated.

Using the  $\mathbb{L}$ -periodicity of this operator, and performing the Bloch transform with respect to the longitudinal variables, we obtain the family of Hamiltonians  $H_{\mathbf{k}}^{(1)} := -\frac{1}{2}\Delta + V$ ,  $\mathbf{k} \in \mathbb{R}^2$ , each  $H_{\mathbf{k}}^{(1)}$  acting on the fiber

$$L_{\mathbf{k}}^2 := \left\{ \psi_{\mathbf{k}} \in L_{\text{loc}}^2(\mathbb{R}^3; \mathbb{C}) \mid \forall \mathbf{R} \in \mathbb{L}, (\tau_{\mathbf{R}}\psi_{\mathbf{k}})(\mathbf{x}, z) = e^{i\mathbf{k} \cdot \mathbf{R}} \psi_{\mathbf{k}}(\mathbf{x}, z), \int_{\Omega \times \mathbb{R}} |\psi_{\mathbf{k}}|^2 < \infty \right\},$$

where  $\Omega \subset \mathbb{R}^2$  is the Wigner-Seitz cell of the lattice  $\mathbb{L}$  (an hexagon with a carbon atom at each of its six vertices). We denote by  $\langle \cdot, \cdot \rangle$  the natural inner product of  $L_{\mathbf{k}}^2$ :

$$\langle \phi_{\mathbf{k}}, \psi_{\mathbf{k}} \rangle := \int_{\Omega \times \mathbb{R}} \overline{\phi_{\mathbf{k}}(\mathbf{x}, z)} \psi_{\mathbf{k}}(\mathbf{x}, z) d\mathbf{x} dz.$$

We also denote by  $L_{\text{per}}^2 := L_{\mathbf{0}}^2$  the space of  $\mathbb{L}$ -periodic functions that are square-integrable on  $\Omega \times \mathbb{R}$ . The map  $\mathbf{k} \mapsto H_{\mathbf{k}}^{(1)}$  is  $\mathbb{L}^*$ -periodic, where  $\mathbb{L}^*$  is the dual lattice of  $\mathbb{L}$ . Explicitly,

$$\mathbb{L}^* = \mathbf{a}_1^* \mathbb{Z} + \mathbf{a}_2^* \mathbb{Z} \quad \text{with} \quad \mathbf{a}_1^* = \sqrt{3}k_D \begin{pmatrix} \sqrt{3}/2 \\ -1/2 \end{pmatrix} \quad \text{and} \quad \mathbf{a}_2^* = \sqrt{3}k_D \begin{pmatrix} \sqrt{3}/2 \\ 1/2 \end{pmatrix},$$

where  $k_D := \frac{4\pi}{3a_0}$ . The symmetry properties of the potential  $V$  and the Laplace operator lead in particular to

$$\mathcal{C}H_{\mathbf{k}}\mathcal{C}^* = H_{-\mathbf{k}}, \quad \mathcal{P}H_{\mathbf{k}}\mathcal{P}^* = H_{-\mathbf{k}}, \quad \mathfrak{R}H_{\mathbf{k}}\mathfrak{R} = H_{M\mathbf{k}}, \quad \text{and} \quad \mathcal{R}_{\frac{2\pi}{3}}H_{\mathbf{k}}\mathcal{R}_{\frac{2\pi}{3}}^* = H_{R_{\frac{2\pi}{3}}\mathbf{k}},$$

where the operators  $\mathcal{P}, \mathfrak{R}$  and  $\mathcal{R}_{\frac{2\pi}{3}}$  (resp.  $\mathcal{C}$ ) are here considered as unitary (resp. anti-unitary) operators between two different fibers of the Bloch bundle. The matrix  $M := \begin{pmatrix} 1 & 0 \\ 0 & -1 \end{pmatrix}$  represents the in-plane mirror symmetry with respect to  $x_1$ -axis. In particular, at the Dirac point

$$\mathbf{K} := -\frac{1}{3}(\mathbf{a}_1^* + \mathbf{a}_2^*) = k_D \begin{pmatrix} -1 \\ 0 \end{pmatrix}, \quad (5)$$

which satisfies  $R_{\frac{2\pi}{3}}\mathbf{K} = \mathbf{K} \bmod \mathbb{L}^*$  and  $M\mathbf{K} = \mathbf{K}$ , the operator  $H_{\mathbf{K}}$  commutes with the operators  $(\mathcal{C}\mathcal{P})$ ,  $\mathfrak{R}$ ,  $\mathcal{S}$  and  $\mathcal{R}_{\frac{2\pi}{3}}$ .

**Remark 1.** *Instead of the point  $\mathbf{K}$  defined in (5), we could choose any of the other five vertices of the graphene first Brillouin zone. We made this particular choice in order to derive continuum models for twisted bilayer graphene with the exact same mathematical structure as those in e.g. [6, 27]. Other choices would have lead to unitary equivalent models less easy to compare with the models in [6, 27]. The same objective governed the choice of the scaling factor  $\varepsilon_\theta$  in (13), the  $\mathbf{q}$ -vectors in (40)-(42), and the symmetry-adapted Bloch functions  $\Phi_1$  and  $\Phi_2$  at the Dirac point  $\mathbf{K}$  used in the parameterization of our reduced model. Although the construction of these functions lays on classical arguments (see in particular [16]), we will detail it here for the sake of completeness, but also, and mainly, because we need to choose the gauge appropriately.*

Since  $\mathcal{R}_{\frac{2\pi}{3}}$  satisfies  $\mathcal{R}_{\frac{2\pi}{3}}^3 = \mathbb{I}_3$ , the eigenvalues of this operator are 1,  $\omega := e^{i2\pi/3}$  and  $\omega^2 = \bar{\omega}$ . Let us decompose  $L_{\mathbf{K}}^2$  accordingly as

$$L_{\mathbf{K}}^2 = L_{\mathbf{K},1}^2 \oplus L_{\mathbf{K},\omega}^2 \oplus L_{\mathbf{K},\bar{\omega}}^2.$$

Let  $\mu$  be an eigenvalue of multiplicity 1 of  $H_{\mathbf{K},\omega}^{(1)}$ , the restriction of  $H_{\mathbf{K}}^{(1)}$  to  $L_{\mathbf{K},\omega}^2$ , and let  $\widetilde{\Phi}_1 \in L_{\mathbf{K},\omega}^2$  be a corresponding normalized eigenvector. Since

$$\mathfrak{R}\mathcal{R}_\theta = \mathcal{R}_{-\theta}\mathfrak{R}, \quad \text{and} \quad (\mathcal{CP})\mathcal{R}_\theta = \mathcal{R}_\theta(\mathcal{CP}),$$

the function  $\mathfrak{R}\mathcal{CP}\widetilde{\Phi}_1$  also belongs to  $L_{\mathbf{K},\omega}^2$ , and is an eigenvector of  $H_{\mathbf{K},\omega}^{(1)}$  for the same eigenvalue  $\mu$ . As a consequence, it is collinear to  $\widetilde{\Phi}_1$ , so that there is  $\alpha \in \mathbb{R}$  for which

$$\mathfrak{R}\mathcal{CP}\widetilde{\Phi}_1 = e^{i\alpha}\widetilde{\Phi}_1.$$

We set

$$\Phi_1 = i^\sigma e^{i\alpha/2} \widetilde{\Phi}_1 \in L_{\mathbf{K},\omega}^2, \quad \text{and} \quad \Phi_2 = (\mathcal{CP})\Phi_1 \in L_{\mathbf{K},\bar{\omega}}^2, \quad (6)$$

where  $\sigma \in \{0, 1\}$  will be chosen later. Since  $\Phi_1 \in L_{\mathbf{K},\omega}^2$  while  $\Phi_2 \in L_{\mathbf{K},\bar{\omega}}^2$ , the functions  $\Phi_1$  and  $\Phi_2$  are orthogonal, and  $\mu$  is an eigenvalue of  $H_{\mathbf{K}}^{(1)}$  of multiplicity at least 2. This happens in particular at the Fermi-level  $\mu = \mu_F$  of uncharged graphene, which is a two-fold degenerate eigenvalue of  $H_{\mathbf{K}}$ . In what follows,  $\Phi_1$  and  $\Phi_2$  are normalized eigenfunctions of  $H_{\mathbf{K}}$  (for the eigenvalue  $\mu_F$ ),  $\mathcal{R}_{\frac{2\pi}{3}}$  (for the eigenvalues  $\omega$  and  $\bar{\omega}$  respectively), and  $\mathfrak{R}\mathcal{CP}$  (for the eigenvalue  $(-1)^\sigma$ ) constructed as above. The valence orbitals of graphene belong to a  $\pi$ -shell, hence we also have

$$\Phi_1(\mathbf{x}, -z) = -\Phi_1(\mathbf{x}, z), \quad \text{and} \quad \Phi_2(\mathbf{x}, -z) = -\Phi_2(\mathbf{x}, z). \quad (7)$$

We now define the Fermi velocity. For  $j, j' \in \{1, 2\}$ , we introduce the vector

$$\mathbf{m}_{jj'} := \langle \Phi_j, -i\nabla_{\mathbf{x}}\Phi_{j'} \rangle.$$

Since  $(-i\nabla_{\mathbf{x}}\Phi_1)(R_{\frac{2\pi}{3}}^*\mathbf{x}, z) = R_{\frac{2\pi}{3}}^*[( -i\nabla_{\mathbf{x}})(\mathcal{R}_{\frac{2\pi}{3}}\Phi_1)](\mathbf{x}, z)$  and  $\mathcal{R}_{\frac{2\pi}{3}}\Phi_1 = \omega\Phi_1$ , we have

$$\begin{aligned} \mathbf{m}_{11} &= \int_{\Omega \times \mathbb{R}} \overline{\Phi_1(\mathbf{x}, z)} (-i\nabla_{\mathbf{x}}\Phi_1)(\mathbf{x}, z) d\mathbf{x} dz = \int_{\Omega \times \mathbb{R}} \overline{\Phi_1(R_{\frac{2\pi}{3}}^*\mathbf{x}, z)} (-i\nabla_{\mathbf{x}}\Phi_1)(R_{\frac{2\pi}{3}}^*\mathbf{x}, z) d\mathbf{x} dz \\ &= \langle \mathcal{R}_{\frac{2\pi}{3}}\Phi_1, R_{\frac{2\pi}{3}}^*(-i\nabla_{\mathbf{x}})(\mathcal{R}_{\frac{2\pi}{3}}\Phi_1) \rangle = R_{\frac{2\pi}{3}}^* \langle \omega\Phi_1, -i\nabla_{\mathbf{x}}(\omega\Phi_1) \rangle = R_{\frac{2\pi}{3}}^* \mathbf{m}_{11}. \end{aligned} \quad (8)$$

This implies that  $\mathbf{m}_{11} = (0, 0)^T$ . Likewise, we obtain  $\mathbf{m}_{22} = (0, 0)^T$ . A similar calculation using  $\mathcal{R}_{\frac{2\pi}{3}}\Phi_2 = \bar{\omega}\Phi_2$  leads to  $\mathbf{m}_{12} = \omega R_{\frac{2\pi}{3}}^* \mathbf{m}_{12}$ , which shows that  $\mathbf{m}_{12}$  belongs to the

eigenspace of  $R_{\frac{2\pi}{3}}$  associated with the eigenvalue  $\omega$ . We deduce that it is collinear to  $(-1, i)^T$ : there exists  $v_F \in \mathbb{C}$  so that

$$\langle \Phi_1, (-i\nabla_{\mathbf{x}})\Phi_1 \rangle = \langle \Phi_2, (-i\nabla_{\mathbf{x}})\Phi_2 \rangle = \begin{pmatrix} 0 \\ 0 \end{pmatrix}, \quad \text{and} \quad \langle \Phi_1, (-i\nabla_{\mathbf{x}})\Phi_2 \rangle = v_F \begin{pmatrix} -1 \\ i \end{pmatrix}. \quad (9)$$

Using that  $\Re(-i\partial_{x_1}) = (-i\partial_{x_1})\Re$  and  $\Re\Phi_1 = (-1)^\sigma\Phi_2$ , we have

$$v_F = \langle \Phi_1, (-i\partial_{x_1})\Phi_2 \rangle = \langle \Re\Phi_1, \Re(-i\partial_{x_1})\Phi_2 \rangle = (-1)^{2\sigma} \langle \Phi_2, (-i\partial_{x_1})\Phi_1 \rangle = \overline{v_F},$$

hence  $v_F \in \mathbb{R}$ . Changing  $\sigma$  into  $(1-\sigma)$  changes  $v_F$  into  $-v_F$ , and we can therefore choose  $\sigma$  so that  $v_F \geq 0$ . Numerical simulations give  $\sigma = 1$ . The quantity  $v_F$ , which turns out to be (strictly) positive for graphene, is the single-layer graphene Fermi velocity. It follows from perturbation theory that it is equal to the slope of the Dirac cone at  $\mathbf{K}$ .

We finally denote by  $u_1$  and  $u_2$  the unique functions in  $L^2_{\text{per}}$  such that

$$\Phi_1(\mathbf{x}, z) = e^{i\mathbf{K}\cdot\mathbf{x}}u_1(\mathbf{x}, z), \quad \text{and} \quad \Phi_2(\mathbf{x}, z) = e^{i\mathbf{K}\cdot\mathbf{x}}u_2(\mathbf{x}, z). \quad (10)$$

It results from the above arguments that the functions  $u_1$  and  $u_2$  satisfy the normalization conditions

$$\langle u_j, u_{j'} \rangle = \delta_{jj'},$$

and the symmetry properties

$$(\mathcal{R}_{\frac{2\pi}{3}}u_j)(\mathbf{x}, z) = \omega^j e^{i(1-R_{\frac{2\pi}{3}})\mathbf{K}\cdot\mathbf{x}}u_j(\mathbf{x}, z), \quad (11)$$

$$u_j(\mathbf{x}, -z) = -u_j(\mathbf{x}, z), \quad u_2(\mathbf{x}, z) = \overline{u_1(-\mathbf{x}, z)}, \quad u_2(x_1, x_2, z) = u_1(x_1, -x_2, z). \quad (12)$$

The exact same arguments hold for the other valley, corresponding to  $\mathbf{K}' := -\mathbf{K}$ .

## 2.2 Kohn-Sham model for TBG

We now consider two parallel layers of graphene, separated by a distance  $d > 0$ , and with a twist angle  $\theta$  between the two. More precisely, we first place the top layer in the plane  $z = \frac{d}{2}$  and the bottom layer in the plane  $z = -\frac{d}{2}$  in AA stacking, and then rotate the top layer by  $\theta/2$  and the bottom layer by  $-\theta/2$  around the  $z$ -axis, placing the origin at the center of a carbon hexagon. In what follows, we set for clarity

$$c_\theta := \cos \frac{\theta}{2} \quad \text{and} \quad \varepsilon_\theta := 2 \sin \frac{\theta}{2}. \quad (13)$$

Note that  $\varepsilon_\theta \sim \theta$  in the small-angle limit. We introduce the unitary operator on  $L^2(\mathbb{R}^3; \mathbb{C})$  defined by

$$(U_{d,\theta}f)(\mathbf{x}, z) := f\left(R_{\theta/2}^*\mathbf{x}, z - \frac{d}{2}\right) = f\left(c_\theta\mathbf{x} - \frac{1}{2}\varepsilon_\theta J\mathbf{x}, z - \frac{d}{2}\right). \quad (14)$$

The inverse of  $U_{d,\theta}$  is  $U_{d,\theta}^{-1} = U_{d,\theta}^* = U_{-d,-\theta}$ . In a non-interacting model (that is without taking into account the electron-electron interaction), the external potential of the twisted bilayer graphene would be of the form  $U_{d,\theta}V + U_{d,\theta}^{-1}V$ , each component  $U_{d,\theta}^{\pm 1}V$  representing a layer of graphene shifted by  $\pm \frac{d}{2}\mathbf{e}_z$ , and twisted by an angle  $\pm \theta/2$ . For a mean-field model with interacting electrons, the expression  $U_{d,\theta}V + U_{d,\theta}^{-1}V$  is only valid in the limit  $d \rightarrow \infty$ . For  $d \approx 3.4 \text{ \AA} \approx 6.5 \text{ bohr}$  (recall that the carbon-carbon distance is  $a = 2.68 \text{ bohr}$ ), the experimental interlayer distance in TBG, a better approximation is obtained as follows (see

also [28]). For  $\mathbf{y} \in \Omega$  a disregistry vector, we denote by  $V_{d,\mathbf{y}}^{(2)}$  the mean-field Kohn-Sham potential for the configuration where the two layers are aligned (no twist angle) and the top one shifted by  $\mathbf{y}$  in the longitudinal direction. We then set

$$V_{\text{int},d,\mathbf{y}}(z) := \oint_{\Omega} \left( V_{d,\mathbf{y}}^{(2)}(\mathbf{x}, z) - V(\mathbf{x}, z + \frac{d}{2}) - V(\mathbf{x} - \mathbf{y}, z - \frac{d}{2}) \right) d\mathbf{x}, \quad (15)$$

and

$$V_{\text{int},d}(z) := \oint_{\Omega} V_{\text{int},d,\mathbf{y}}(z) d\mathbf{y}, \quad (16)$$

where  $\oint_{\Omega} := |\Omega|^{-1} \int_{\Omega}$ . In other words,  $V_{\text{int},d}$  is the mismatch between the interacting Kohn-Sham potential and the non-interacting one, averaged over all possible disregistries  $\mathbf{y} \in \Omega$ . Note that  $V_{\text{int},d}(z)$  only depends on the  $z$ -variable and satisfies

$$V_{\text{int},d}(-z) = V_{\text{int},d}(z).$$

Our approximate Kohn-Sham potential for the TBG is

$$\boxed{V_{d,\theta}^{(2)}(\mathbf{x}, z) := (U_{d,\theta} V)(\mathbf{x}, z) + (U_{d,\theta}^{-1} V)(\mathbf{x}, z) + V_{\text{int},d}(z).} \quad (17)$$

**Remark 2.** For twist angles  $\theta$  giving rise to a periodic structure at the moiré scale, that is for the countable set of twist angles  $\theta$  such that

$$\cos \theta = \frac{3n^2 + 3nr + r^2/2}{3n^2 + 3nr + r^2}, \quad \text{for } n, r \text{ positive coprime integers,}$$

the TBG Kohn-Sham potential is a mathematically well-defined moiré-periodic function, at least within the Hartree or local density approximations. On the other hand, it is not clear how to define a mean-field potential for incommensurate twist angles. This problem actually occurs for all infinite aperiodic systems. For instance, the Hartree ground-state density of an aperiodic disordered (ergodic) crystal has been shown to be a well-defined mathematical object [7], but it is not known whether the Poisson equation defining the Hartree potential has a solution allowing one to define a self-consistent Hartree Hamiltonian. To proceed with the construction of a Kohn-Sham Hamiltonian for TBG, we assume that the TGB Kohn-Sham potential exists and can be approximated by (17).

In what follows, we study the approximate TBG Kohn-Sham Hamiltonian

$$\boxed{H_{d,\theta}^{(2)} := -\frac{1}{2}\Delta + V_{d,\theta}^{(2)}(\mathbf{x}, z)} \quad (18)$$

Our goal is to derive a 2D reduced model describing the low-energy band structure around the Fermi level  $\mu_F$  in the limit of small twist angles.

**Remark 3.** We have  $V_{d,\theta}^{(2)}(\mathbf{x}, z) = v_d(c_\theta \mathbf{x}, \varepsilon_\theta \mathbf{x}, z)$ , with

$$v_d(\mathbf{x}, \mathbf{X}, z) = V(\mathbf{x} - \frac{1}{2}J\mathbf{X}, z - \frac{d}{2}) + V(\mathbf{x} + \frac{1}{2}J\mathbf{X}, z + \frac{d}{2}) + V_{\text{int},d}(z).$$

The potential  $v_d$  is  $\mathbb{L}$ -periodic in the first variable  $\mathbf{x}$ , and  $2J\mathbb{L}$ -periodic in its second variable  $\mathbf{X}$ . The Hamiltonian

$$h_{d,\mathbf{X}} = -\frac{1}{2}\Delta_{\mathbf{x},z} + v_d(\cdot, \mathbf{X}, \cdot) \quad (19)$$

describes an untwisted bilayer graphene with interlayer distance  $d$  and disregistry  $\mathbf{y} = J\mathbf{X}$ . In the limit  $\theta \rightarrow 0$ , we have  $c_\theta \approx 1$  and  $\varepsilon_\theta \ll 1$ , so that the Hamiltonian

$$H_{d,\theta}^{(2)} = -\frac{1}{2}\Delta + v_d(c_\theta \mathbf{x}, \varepsilon_\theta \mathbf{x}, z)$$

has a natural two-scale structure, and can be mathematically studied using powerful tools of adiabatic theory, semiclassical analysis, and homogenization theory.

### 3 Reduced model

We now introduce the additional approximations leading to our reduced model for TBG, present the mathematical structure of this model, comment on its symmetry properties, and discuss its similarities with the BM model. We assume that the potentials  $V$  and  $V_{\text{int}}$  are of class  $C^\infty$ , and we postpone the technical steps of the derivation until Appendix A.

#### 3.1 Variational approximation of low-energy wavepacket dynamics

In order to motivate our approach, we first explain how to implement it in the simpler case of single-layer graphene with Hamiltonian (4). It is well-known that in an energy range close to the Fermi level, electrons and holes propagate as massless Dirac particles. A rigorous mathematical formulation of this property was established by Fefferman and Weinstein [16]. They considered the 2D time-dependent Schrödinger equation

$$i\partial_t\psi(t, \mathbf{x}) = -\Delta\psi(t, \mathbf{x}) + v(\mathbf{x})\psi(t, \mathbf{x}), \quad \psi(0, \mathbf{x}) = \psi_0(\mathbf{x}), \quad (t, \mathbf{x}) \in \mathbb{R} \times \mathbb{R}^2,$$

where the potential  $v : \mathbb{R}^2 \rightarrow \mathbb{R}$  has the honeycomb symmetry (p6m wallpaper group), but their argument can be easily extended to the 3D time-dependent Schrödinger equation

$$i\partial_t\psi(t, \mathbf{r}) = (H^{(1)} - \mu_F)\psi(t, \mathbf{r}), \quad \psi(0, \mathbf{r}) = \psi_0(\mathbf{r}), \quad (t, \mathbf{r}) \in \mathbb{R} \times \mathbb{R}^3, \quad (20)$$

where the Hamiltonian  $H^{(1)}$  is the single-layer graphene Kohn-Sham Hamiltonian defined in (4). We denote by  $\mathcal{S}(\mathbb{R}^2; \mathbb{C}^n)$  the Schwartz space of  $\mathbb{C}^n$ -valued functions on  $\mathbb{R}^2$  and recall that  $\Phi_1$  and  $\Phi_2$  are the Bloch waves of graphene of energy  $\mu_F$  at the Dirac point  $\mathbf{K}$ . Loosely speaking, the main result of [16] states that for well-prepared initial data

$$\psi_0^\varepsilon(\mathbf{r}) = \sum_{j=1}^2 \varepsilon \alpha_j^0(\varepsilon \mathbf{x}) \Phi_j(\mathbf{x}, z), \quad \text{with } \mathbf{r} = (\mathbf{x}, z) \in \mathbb{R}^3, \quad (21)$$

where  $\alpha^0 \in \mathcal{S}(\mathbb{R}^2; \mathbb{C}^2)$ , the solution  $\psi^\varepsilon$  to (20) with  $\psi_0 = \psi_0^\varepsilon$  can be written as

$$\psi^\varepsilon(t, \mathbf{r}) = \sum_{j=1}^2 \varepsilon \alpha_j(\varepsilon t, \varepsilon \mathbf{x}) \Phi_j(\mathbf{x}, z) + \text{h.o.t.},$$

where  $\alpha : \mathbb{R}_+ \times \mathbb{R}^2 \rightarrow \mathbb{C}^2$  satisfies the massless Dirac equation

$$i\partial_\tau \alpha = v_F \boldsymbol{\sigma} \cdot (-i\nabla) \alpha, \quad \alpha(\tau = 0) = \alpha^0. \quad (22)$$

The parameter  $v_F$  is the Fermi velocity of graphene defined in (9) and

$$\boldsymbol{\sigma} \cdot (-i\nabla) = \sigma_1 \cdot (-i\partial_{x_1}) + \sigma_2 \cdot (-i\partial_{x_2}) = \begin{pmatrix} 0 & -i\partial_{x_1} - \partial_{x_2} \\ -i\partial_{x_1} + \partial_{x_2} & 0 \end{pmatrix}.$$

The initial data (21) describes a wave-packet spectrally concentrated around the Fermi level  $\mu_F$  and localized in momentum space in the  $\mathbf{K}$ -valley. The same holds true for the  $\mathbf{K}'$ -valley.

Formally, the equation (22) can be obtained by (i) rescaling the time variable by a factor  $\varepsilon$ , (ii) considering the variational approximation of the time-dependent Schrödinger equation (20) in the two-scale approximation space

$$\mathcal{X}_\varepsilon := \{(\alpha : \Phi)_\varepsilon, \alpha \in \mathcal{S}(\mathbb{R}^2; \mathbb{C}^2)\} \subset H^1(\mathbb{R}^3; \mathbb{C}),$$



with

$$(\alpha : \Phi)_\varepsilon(\mathbf{r}) := \sum_{j \in \{1,2\}} \alpha_j(\varepsilon \mathbf{x}) \Phi_j(\mathbf{x}, z),$$

and (iii) letting  $\varepsilon$  go to zero. Let us explain this point in more details. First, we observe that the space  $\mathcal{X}_\varepsilon$  is, in fact, independent of  $\varepsilon$ , but we nevertheless add the subscript  $\varepsilon$  to emphasize the two-scale character of the approximation. Note that the initial data  $\psi_0^\varepsilon$  is of the form  $\psi_0^\varepsilon = (\alpha_0 : \Phi)_\varepsilon$  for a fixed initial envelope function  $\alpha_0 = \mathcal{S}(\mathbb{R}^2; \mathbb{C}^2)$ .

After rescaling the time variable, the variational approximation of (20) in  $\mathcal{X}_\varepsilon$  consists in seeking  $\alpha \in C^1(\mathbb{R}_+; \mathcal{S}(\mathbb{R}^2; \mathbb{C}^2))$  such that for all  $\tilde{\alpha} \in \mathcal{S}(\mathbb{R}^2; \mathbb{C}^2)$ ,

$$i \frac{d}{dt} \langle (\tilde{\alpha} : \Phi)_\varepsilon, (\alpha(\varepsilon t) : \Phi)_\varepsilon \rangle = \left\langle (\tilde{\alpha} : \Phi)_\varepsilon, (H^{(1)} - \mu_F)(\alpha(\varepsilon t) : \Phi)_\varepsilon \right\rangle. \quad (23)$$

Using the identity (with obvious notations)

$$\left[ (H^{(1)} - \mu_F)(\alpha : \Phi)_\varepsilon \right] = \varepsilon^2 \left( (-\tfrac{1}{2} \Delta \alpha) : \Phi \right)_\varepsilon + \varepsilon \left( (-i \nabla \alpha) : (-i \nabla_{\mathbf{x}} \Phi_{j'}) \right)_\varepsilon,$$

and the change of variable  $\mathbf{X} = \varepsilon \mathbf{x}$  and  $\tau = \varepsilon t$ , we get

$$\begin{aligned} & i \sum_{j,j'=1}^2 \int_{\mathbb{R}^3} \overline{\tilde{\alpha}_j(\mathbf{X})} \frac{\partial}{\partial \tau} \alpha_{j'}(\tau, \mathbf{X}) \overline{\Phi_j(\varepsilon^{-1} \mathbf{X}, z)} \Phi_{j'}(\varepsilon^{-1} \mathbf{X}, z) d\mathbf{X} dz \\ &= \varepsilon \sum_{j,j'=1}^2 \int_{\mathbb{R}^3} \overline{\tilde{\alpha}_j(\mathbf{X})} \left( -\tfrac{1}{2} \Delta \alpha_{j'}(\tau, \mathbf{X}) \right) \overline{\Phi_j(\varepsilon^{-1} \mathbf{X}, z)} \Phi_{j'}(\varepsilon^{-1} \mathbf{X}, z) d\mathbf{X} dz \\ &+ \sum_{j,j'=1}^2 \int_{\mathbb{R}^3} \overline{\tilde{\alpha}_j(\mathbf{X})} (-i \nabla \alpha_{j'}(\tau, \mathbf{X})) \cdot \overline{\Phi_j(\varepsilon^{-1} \mathbf{X}, z)} (-i \nabla_{\mathbf{x}} \Phi_{j'})(\varepsilon^{-1} \mathbf{X}, z) d\mathbf{X} dz. \end{aligned} \quad (24)$$

Lastly, using the orthonormality condition  $\langle \Phi_j, \Phi_{j'} \rangle = \delta_{jj'}$ , the relations (9), and the fact that for all  $\beta \in \mathcal{S}(\mathbb{R}^3; \mathbb{C})$  and  $\Xi \in L^1_{\text{per}}$ , we have (see Lemma 1 below)

$$\int_{\mathbb{R}^3} \beta(\mathbf{X}) \Xi(\varepsilon^{-1} \mathbf{X}, z) d\mathbf{X} dz \xrightarrow{\varepsilon \rightarrow 0} \left( \int_{\mathbb{R}^3} \beta(\mathbf{X}) d\mathbf{X} \right) \left( \frac{1}{|\Omega|} \int_{\Omega \times \mathbb{R}} \Xi(\mathbf{x}, z) d\mathbf{x} dz \right),$$

we obtain by letting  $\varepsilon$  go to zero in (24) for fixed  $\alpha$  and  $\tilde{\alpha}$ ,

$$i \sum_{j=1}^2 \int_{\mathbb{R}^2} \overline{\tilde{\alpha}_j(\mathbf{X})} \frac{\partial}{\partial \tau} \alpha_j(\tau, \mathbf{X}) d\mathbf{X} = v_F \sum_{j=1}^2 \int_{\mathbb{R}^2} \overline{\tilde{\alpha}_j(\mathbf{X})} [\boldsymbol{\sigma} \cdot (-i \nabla \alpha)]_j(\tau, \mathbf{X}) d\mathbf{X}, \quad (25)$$

which is nothing but the variational formulation of the massless Dirac equation (22).

In order to derive an effective model describing the low-energy excitations in TBG in the small twist angle limit (in the  $\mathbf{K}$ -valley), we adopt a similar strategy. Starting from the approximate Kohn-Sham operator  $H_{d,\theta}^{(2)}$ , we consider the time-dependent Schrödinger equation

$$i \partial_t \Psi(t, \mathbf{r}) = (H_{d,\theta}^{(2)} - \mu_F) \Psi(t, \mathbf{r}), \quad \Psi(0, \mathbf{r}) = \Psi_0(\mathbf{r}), \quad (t, \mathbf{r}) \in \mathbb{R} \times \mathbb{R}^3, \quad (26)$$

and the two-scale approximation space

$$\mathcal{X}_{d,\theta} := \{(\alpha : \Phi)_{d,\theta}, \alpha \in \mathcal{S}(\mathbb{R}^2; \mathbb{C}^4)\} \subset H^1(\mathbb{R}^3; \mathbb{C}), \quad (27)$$

where

$$(\alpha : \Phi)_{d,\theta}(\mathbf{x}, z) := \sum_{\substack{\eta \in \{\pm 1\} \\ j \in \{1, 2\}}} \alpha_{\eta,j}(\varepsilon_\theta \mathbf{x}) (U_{d,\theta}^\eta \Phi_j)(\mathbf{x}, z).$$

The trial functions in  $\mathcal{X}_{d,\theta}$  are thus linear combinations of four wave-packets, each of these wave-packets consisting of an envelope function oscillating at the moiré scale  $\varepsilon_\theta^{-1}$  multiplied by one of the two (translated and rotated) Bloch waves  $\Phi_1$  or  $\Phi_2$  of one of the two layers. In contrast with the single-layer graphene case, both the TBG approximation subspace  $\mathcal{X}_{d,\theta}$  and Hamiltonian  $H_{d,\theta}^{(2)}$  depend on the small parameter  $\theta$ .

The variational approximation of (26) in the space  $\mathcal{X}_{d,\theta}$  consists in seeking a function  $\alpha \in C^1(\mathbb{R}_+; \mathcal{S}(\mathbb{R}^2; \mathbb{C}^4))$  such that for all  $\tilde{\alpha} \in \mathcal{S}(\mathbb{R}^2; \mathbb{C}^4)$ ,

$$\begin{cases} i \frac{d}{dt} \langle (\tilde{\alpha} : \Phi)_{d,\theta}, (\alpha(\varepsilon_\theta t) : \Phi)_{d,\theta} \rangle = \langle (\tilde{\alpha} : \Phi)_{d,\theta}, (H_{d,\theta}^{(2)} - \mu_F)(\alpha(\varepsilon_\theta t) : \Phi)_{d,\theta} \rangle, \\ \alpha(\tau = 0, \mathbf{x}) = \alpha^0(\mathbf{x}). \end{cases} \quad (28)$$

**Remark 4.** Alternatively, we could consider the two-scale functions of the form

$$\sum_{j=1}^4 \alpha_j(\varepsilon_\theta \mathbf{x}) \Phi_j^{d,\varepsilon_\theta \mathbf{x}}(c_\theta \mathbf{x}, z) \quad (29)$$

where, for all  $\mathbf{X} \in \mathbb{R}^2$ , the functions  $(\Phi_j^{d,\mathbf{X}})_{1 \leq j \leq 4}$  span the same four-dimensional subspace of  $L_{\mathbf{K}}^2$  as the eigenfunctions of the Bloch fiber  $[h_{d,\mathbf{X}}]_{\mathbf{K}}$  of the operator  $h_{d,\mathbf{X}}$  defined in (19) associated with the four eigenvalues close to  $\mu_F$ . However, since the two layers are weakly interacting, the spaces spanned by  $(\Phi_j^{d,\varepsilon_\theta \mathbf{x}}(c_\theta \mathbf{x}, z))_{1 \leq j \leq 4}$  and  $(U_{d,\theta}^\eta \Phi_j)(\mathbf{x}, z)_{\eta=\pm 1, j=1,2}$  are equal at leading order and we therefore expect the two approaches to give similar results.

### 3.2 Formulation of the reduced model

It follows from tedious calculations detailed in Appendix A that if we let  $\theta$  go to zero in (28) for fixed trial functions  $\tilde{\alpha}$  and  $\alpha_{d,\theta}$ , we obtain the asymptotic equality

$$i \frac{d}{d\tau} \langle \tilde{\alpha}, \mathcal{S}_d \alpha_{d,\theta}(\tau) \rangle = \langle \tilde{\alpha}, \mathcal{H}_{d,\theta} \alpha_{d,\theta}(\tau) \rangle + O(\varepsilon_\theta^\infty), \quad (30)$$

where the overlap operator  $\mathcal{S}_d$  and the Hamiltonian operator  $\mathcal{H}_{d,\theta}$  are operators on  $L^2(\mathbb{R}^2; \mathbb{C}^4)$  defined by

$$\boxed{\mathcal{S}_d = \begin{pmatrix} \mathbb{I}_2 & \Sigma_d(\mathbf{X}) \\ \Sigma_d^*(\mathbf{X}) & \mathbb{I}_2 \end{pmatrix} \quad \text{and} \quad \mathcal{H}_{d,\theta} = \varepsilon_\theta^{-1} \mathcal{V}_d + c_\theta T_d + \varepsilon_\theta T_d^{(1)}} \quad (31)$$

where the three operators  $\mathcal{V}_d$ ,  $T_d$ , and  $T_d^{(1)}$  are of the form

$$\begin{aligned} \mathcal{V}_d &= \begin{pmatrix} \mathbb{W}_d^+(\mathbf{X}) & \mathbb{V}_d(\mathbf{X}) \\ \mathbb{V}_d(\mathbf{X})^* & \mathbb{W}_d^-(\mathbf{X}) \end{pmatrix}, \\ T_d &= \begin{pmatrix} v_F \boldsymbol{\sigma} \cdot (-i\nabla) & J(-i\nabla \Sigma_d)(\mathbf{X}) \cdot (-i\nabla) \\ J(-i\nabla \Sigma_d^*)(\mathbf{X}) \cdot (-i\nabla) & v_F \boldsymbol{\sigma} \cdot (-i\nabla) \end{pmatrix}, \\ T_d^{(1)} &= -\frac{1}{2} \operatorname{div}(\mathcal{S}_d(\mathbf{X}) \nabla \bullet) + \frac{1}{2} \begin{pmatrix} -v_F \boldsymbol{\sigma} \cdot J(-i\nabla) & 0 \\ 0 & v_F \boldsymbol{\sigma} \cdot J(-i\nabla) \end{pmatrix}. \end{aligned} \quad (32)$$

The matrix-valued functions  $\Sigma_d(\mathbf{X})$ ,  $\mathbb{V}_d(\mathbf{X})$  and  $\mathbb{W}_d(\mathbf{X})$  are given by (recall that  $u_j$  is the periodic part of  $\Phi_j$ , see Eq. (10))

$$[\Sigma_d(\mathbf{X})]_{jj'} := e^{-iJ\mathbf{K}\cdot\mathbf{X}}((u_j, u_{j'}))_d^{+-}(\mathbf{X}), \quad (33)$$

$$[\mathbb{V}_d(\mathbf{X})]_{jj'} := e^{-iJ\mathbf{K}\cdot\mathbf{X}}((V + V_{\text{int},d}(\cdot + \frac{d}{2})) u_j, u_{j'})_d^{+-}(\mathbf{X}), \quad (34)$$

$$[\mathbb{W}_d^\pm(\mathbf{X})]_{jj'} := ((u_j \bar{u}_{j'}, V))_d^{\pm\mp}(\mathbf{X}) + (W_{\text{int},d}^\pm)_{jj'}, \quad (35)$$

where for all  $f, g \in L_{\text{per}}^2$ ,

$$((f, g))_d^{\eta\eta'}(\mathbf{X}) := \int_{\Omega \times \mathbb{R}} \overline{f(\mathbf{x} - \eta \frac{1}{2} J\mathbf{X}, z - \eta \frac{d}{2})} g(\mathbf{x} - \eta' \frac{1}{2} J\mathbf{X}, z - \eta' \frac{d}{2}) d\mathbf{x} dz, \quad (36)$$

and where

$$(W_{\text{int},d}^\pm)_{jj'} := \int_{\Omega \times \mathbb{R}} (\bar{u}_j u_{j'})(\mathbf{x}, z \mp \frac{d}{2}) V_{\text{int},d}(z) d\mathbf{x} dz. \quad (37)$$

Note that the quantity  $((f, g))_d^{+-}$  in (36) can be rewritten as a convolution product on the cylinder  $\Omega \times \mathbb{R} \equiv \mathbb{R}^2/\mathbb{L} \times \mathbb{R}$ :

$$((f, g))_d^{+-} = \int_{\Omega \times \mathbb{R}} \overline{f(\mathbf{x} - J\mathbf{X}, z - d)} g(\mathbf{x}, z) d\mathbf{x} dz =: ((\mathcal{CPS}f) * g)(J\mathbf{X}, d). \quad (38)$$

In view of their expressions, it is not obvious that the operators  $\mathcal{V}_d$  and  $T_d$  (hence  $\mathcal{H}_{d,\theta}$ ) are self-adjoint on  $L^2(\mathbb{R}^2; \mathbb{C}^4)$ . It is however the case. For instance, it is easy to see that  $((u, v))_d^{+-}(\mathbf{X}) = ((\bar{u}, \bar{v}))_d^{+-}(\mathbf{X})$ , which proves that the matrices  $\mathbb{W}_d^+(\mathbf{X})$  and  $\mathbb{W}_d^-(\mathbf{X})$  are Hermitian (hence  $\mathcal{V}_d$  is self-adjoint). In addition, from the equality,  $\text{div} J\nabla = -\partial_{x_1 x_2}^2 + \partial_{x_2 x_1}^2 = 0$ , we see that the operator  $T_d$  is self-adjoint as well.

The asymptotic equality (30) leads us to introduce the following effective model for the propagation of low-energy wave-packets in TBG:

$$i \frac{\partial}{\partial \tau} (\mathcal{S}_d \alpha_{d,\theta})(\tau, \mathbf{X}) = (\mathcal{H}_{d,\theta} \alpha_{d,\theta})(\tau, \mathbf{X}). \quad (39)$$

At this stage, we have kept all the terms in  $\mathcal{S}_d$  and  $\mathcal{H}_{d,\theta}$ , and only thrown away the remainders of order  $\varepsilon_\theta^\infty$ . Indeed,  $\varepsilon_\theta$  should not be considered as the only small parameter in this problem. The interlayer coupling is also small, hence the operator  $\mathcal{V}_d$  can be considered to be small as well. The interplay between the two parameters  $\varepsilon_\theta$  and  $w$  (the interlayer characteristic interaction energy) is subtle and will be explored in a future work.

**Remark 5.** *It is well established that atomic relaxation plays a key role in the electronic properties of TBG (see e.g. [24] and references therein). Our reduced model (39) has been derived mathematically for an unrelaxed configuration, but it can be extended to take both in-plane and out-of-plane relaxation. Assuming that the atomic displacement fields of the two layers at the moiré scale are known [12, 14], they can be used to construct fields  $\zeta : \mathbb{R}^2 \rightarrow \mathbb{R}^2$  and  $\delta : \mathbb{R}^2 \rightarrow \mathbb{R}$  describing respectively the modifications of the local disregistry and interlayer distance, giving rise to modified Hamiltonian and overlap operators. For instance, the overlap operator would read*

$$\mathcal{S}_d^{\zeta,\delta} = \begin{pmatrix} \mathbb{I}_2 & \Sigma_{d+\delta(\mathbf{X})}(\mathbf{X} + \zeta(\mathbf{X})) \\ \Sigma_{d+\delta(\mathbf{X})}^*(\mathbf{X} + \zeta(\mathbf{X})) & \mathbb{I}_2 \end{pmatrix}.$$

*The mathematical derivation and numerical simulation of such a model is work in progress.*

### 3.3 Symmetries

We enumerate in this section the symmetries satisfied by the operators  $\mathcal{S}_d$  and  $\mathcal{H}_{d,\theta}$ . There are many ways to obtain these symmetries. One can for instance derive the symmetries of the entries of the operators  $\mathcal{H}_{d,\theta}$  and  $\mathcal{S}_d$  from the ones of  $u_1$ ,  $u_2$ ,  $V$  and  $V_{\text{int}}$  using (33)-(36). This is what we do to identify the translation symmetry group and the symmetries which originate from the averaging process. To identify the other symmetries, we take a different approach: we study the symmetries of the operator  $H_{d,\theta}^{(2)}$  and deduce the ones of  $\mathcal{H}_{d,\theta}$  from the fact that the latter operator is the asymptotic expansion of the former.

#### 3.3.1 Translational covariance

First, we note that, for any functions  $f, g \in L^2_{\text{per}}$ , the maps  $((f, g))_d^{\pm\mp}(\mathbf{X})$  are  $J\mathbb{L}$ -periodic. Indeed, for  $\mathbf{R} \in \mathbb{L}$ , we have

$$((f, g))_d^{+-}(\mathbf{X} - J\mathbf{R}) = \int_{\Omega \times \mathbb{R}} \overline{f\left(\mathbf{x} - \frac{1}{2}J\mathbf{X} + \frac{1}{2}\mathbf{R}, z - \frac{d}{2}\right)} g\left(\mathbf{x} + \frac{1}{2}J\mathbf{X} - \frac{1}{2}\mathbf{R}, z + \frac{d}{2}\right) d\mathbf{x} dz.$$

Making the change of variable  $\mathbf{x}' = \mathbf{x} + \frac{1}{2}\mathbf{R}$ , and recalling that the integrand is  $\mathbb{L}$ -periodic, we obtain

$$\begin{aligned} ((f, g))_d^{+-}(\mathbf{X} - J\mathbf{R}) &= \int_{\Omega \times \mathbb{R}} \overline{f\left(\mathbf{x}' - \frac{1}{2}J\mathbf{X}, z - \frac{d}{2}\right)} g\left(\mathbf{x}' + \frac{1}{2}J\mathbf{X} - \mathbf{R}, z + \frac{d}{2}\right) d\mathbf{x} dz \\ &= \int_{\Omega \times \mathbb{R}} \overline{f\left(\mathbf{x}' - \frac{1}{2}J\mathbf{X}, z - \frac{d}{2}\right)} g\left(\mathbf{x}' + \frac{1}{2}J\mathbf{X}, z + \frac{d}{2}\right) d\mathbf{x} dz = ((f, g))_d^{+-}(\mathbf{X}). \end{aligned}$$

The computation is similar for  $((f, g))_d^{-+}$ . This suggests to introduce the rescaled moiré lattice

$$\boxed{\mathbb{L}_M := J\mathbb{L}}$$

the lattice vectors

$$\mathbf{a}_{1,M} = J\mathbf{a}_1 = a_0 \begin{pmatrix} \sqrt{3}/2 \\ 1/2 \end{pmatrix} \quad \text{and} \quad \mathbf{a}_{2,M} = J\mathbf{a}_2 = a_0 \begin{pmatrix} -\sqrt{3}/2 \\ 1/2 \end{pmatrix},$$

so that  $\mathbb{L}_M = \mathbf{a}_{1,M}\mathbb{Z} + \mathbf{a}_{2,M}\mathbb{Z}$ , and the dual basis

$$\mathbf{a}_{1,M}^* = J\mathbf{a}_1^* = \sqrt{3}k_D \begin{pmatrix} 1/2 \\ \sqrt{3}/2 \end{pmatrix} \quad \text{and} \quad \mathbf{a}_{2,M}^* = J\mathbf{a}_2^* = \sqrt{3}k_D \begin{pmatrix} -1/2 \\ \sqrt{3}/2 \end{pmatrix}.$$

Although the moiré pattern generated by the superposition of two twisted honeycomb lattices is not periodic for a generic twist angle  $\theta$ , it looks  $\varepsilon_\theta^{-1}\mathbb{L}_M$ -periodic at the mesoscopic scale  $\varepsilon_\theta^{-1}$  for  $\theta \ll 1$  (see Fig. 2).

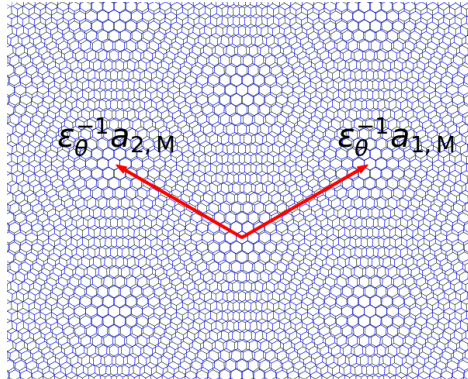


Figure 2: Moiré lattice vectors for twist angle  $\theta \simeq 2.2^\circ$ .

We also introduce the vectors (see Fig. 3)

$$\mathbf{q}_1 := k_D \begin{pmatrix} 0 \\ -1 \end{pmatrix} = \frac{1}{3} (-\mathbf{a}_{1,M}^* - \mathbf{a}_{2,M}^*), \quad (40)$$

$$\mathbf{q}_2 := k_D \begin{pmatrix} \frac{\sqrt{3}}{2} \\ \frac{1}{2} \end{pmatrix} = \frac{1}{3} (2\mathbf{a}_{1,M}^* - \mathbf{a}_{2,M}^*) = R_{\frac{2\pi}{3}} \mathbf{q}_1, \quad (41)$$

$$\mathbf{q}_3 := k_D \begin{pmatrix} -\frac{\sqrt{3}}{2} \\ \frac{1}{2} \end{pmatrix} = \frac{1}{3} (-\mathbf{a}_{1,M}^* + 2\mathbf{a}_{2,M}^*) = R_{\frac{2\pi}{3}} \mathbf{q}_2. \quad (42)$$

These vectors correspond to the  $\mathbf{K}$  valley of the moiré Brillouin zone (compare with (5)). Also, it holds

$$\mathbf{q}_1 = J\mathbf{K}. \quad (43)$$

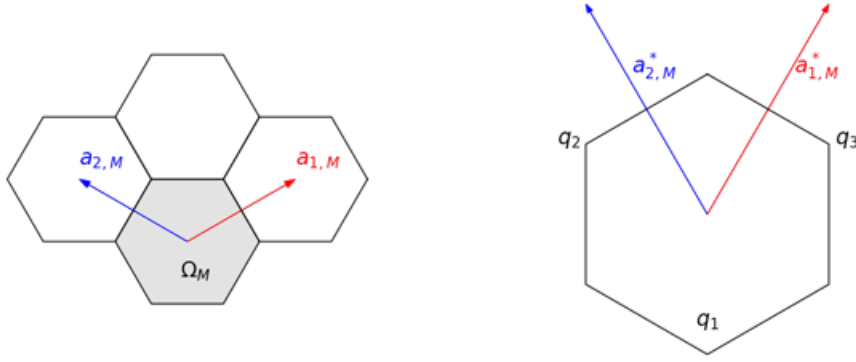


Figure 3: Moiré lattices. Left: the moiré lattice  $\mathbb{L}_M$ . Right: its reciprocal lattice, first moiré Brillouin zone, and the positions of the vectors  $\mathbf{q}_1$ ,  $\mathbf{q}_2$  and  $\mathbf{q}_3$ .

Going back to the matrix elements (33)-(35), we see that the diagonal elements  $\mathbb{W}_d^\pm$  are  $\mathbb{L}_M$ -periodic, and that the off-diagonal elements  $\Sigma_d$  and  $\mathbb{V}_d$  satisfy, for all  $\mathbf{R}_M \in \mathbb{L}_M$ ,

$$\Sigma_d(\mathbf{X} - \mathbf{R}_M) = e^{i\mathbf{q}_1 \cdot \mathbf{R}_M} \Sigma_d(\mathbf{X}), \quad \text{and} \quad \mathbb{V}_d(\mathbf{X} - \mathbf{R}_M) = e^{i\mathbf{q}_1 \cdot \mathbf{R}_M} \mathbb{V}_d(\mathbf{X}). \quad (44)$$

Note that if  $\mathbf{R}_M = m_1 \mathbf{a}_{1,M}^* + m_2 \mathbf{a}_{2,M}^*$ , we have  $e^{i\mathbf{q}_1 \cdot \mathbf{R}_M} = \omega^{2(m_1+m_2)}$  (recall that  $\omega := e^{i\frac{2\pi}{3}}$ ).

### 3.3.2 Symmetries induced by the atomic configuration

We now record the symmetries of the operator induced by the specific atomic configuration of the TBG. These symmetries are valid for all  $d > 0$  and  $\theta > 0$ . First, we note that

$$\mathcal{R}_{\frac{2\pi}{3}} U_{d,\theta} = U_{d,\theta} \mathcal{R}_{\frac{2\pi}{3}}, \quad \mathcal{P} U_{d,\theta} = U_{d,\theta} \mathcal{P}, \quad \mathcal{C} U_{d,\theta} = U_{d,\theta} \mathcal{C}, \quad \text{and} \quad \mathfrak{R} U_{d,\theta} = U_{d,\theta}^* \mathfrak{R}.$$

We easily deduce that, for all  $d > 0$  and all  $\theta \in \mathbb{R}$ , we have

$$\left[ H_{d,\theta}^{(2)}, \mathcal{R}_{\frac{2\pi}{3}} \right] = 0, \quad \left[ H_{d,\theta}^{(2)}, \mathcal{P} \right] = 0, \quad \left[ H_{d,\theta}^{(2)}, \mathcal{C} \right] = 0, \quad \text{and} \quad \left[ H_{d,\theta}^{(2)}, \mathfrak{R} \right] = 0.$$

Let us first focus on the 3-fold rotation symmetry. Using (6), we obtain that, for  $\alpha \in H^1(\mathbb{R}^2, \mathbb{C}^4)$ , we have

$$\mathcal{R}_{\frac{2\pi}{3}}(\alpha : \Phi)_{d,\theta} = \left( (\mathcal{R}_{\frac{2\pi}{3}} \alpha) : (\mathcal{R}_{\frac{2\pi}{3}} \Phi) \right)_{d,\theta} = \left( (\widetilde{\mathcal{R}_{\frac{2\pi}{3}}} \alpha) : \Phi \right)_{d,\theta},$$

where we introduced the unitary operator  $\widetilde{\mathcal{R}_{\frac{2\pi}{3}}} : L^2(\mathbb{R}^2; \mathbb{C}^4) \rightarrow L^2(\mathbb{R}^2; \mathbb{C}^4)$  defined by

$$\widetilde{\mathcal{R}_{\frac{2\pi}{3}}} \begin{pmatrix} \alpha_{+,1} \\ \alpha_{+,2} \\ \alpha_{-,1} \\ \alpha_{-,2} \end{pmatrix} = \mathcal{R}_{\frac{2\pi}{3}} \begin{pmatrix} \omega \alpha_{+,1} \\ \omega^2 \alpha_{+,2} \\ \omega \alpha_{-,1} \\ \omega^2 \alpha_{-,2} \end{pmatrix} = \begin{pmatrix} \omega & 0 & 0 & 0 \\ 0 & \omega^2 & 0 & 0 \\ 0 & 0 & \omega & 0 \\ 0 & 0 & 0 & \omega^2 \end{pmatrix} \mathcal{R}_{\frac{2\pi}{3}} \begin{pmatrix} \alpha_{+,1} \\ \alpha_{+,2} \\ \alpha_{-,1} \\ \alpha_{-,2} \end{pmatrix}.$$

We deduce that

$$\left\langle (\tilde{\alpha} : \Phi)_{d,\theta}, \left( H_{d,\theta}^{(2)} - \mu_F \right) (\alpha : \Phi)_{d,\theta} \right\rangle = \left\langle \left( (\widetilde{\mathcal{R}_{\frac{2\pi}{3}}} \tilde{\alpha}) : \Phi \right)_{d,\theta}, \left( H_{d,\theta}^{(2)} - \mu_F \right) \left( (\widetilde{\mathcal{R}_{\frac{2\pi}{3}}} \alpha) : \Phi \right)_{d,\theta} \right\rangle,$$

and a similar formula for  $\left\langle (\tilde{\alpha} : \Phi)_{d,\theta}, (\alpha : \Phi)_{d,\theta} \right\rangle$ . Hence

$$\left[ \mathcal{S}_d, \widetilde{\mathcal{R}_{\frac{2\pi}{3}}} \right] = 0, \quad \text{and} \quad \left[ \mathcal{H}_{d,\theta}, \widetilde{\mathcal{R}_{\frac{2\pi}{3}}} \right] = 0.$$

These commutation relations give rises to symmetry properties on the entries of  $\mathcal{S}_d$  and  $\mathcal{H}_{d,\theta}$ , in particular for  $\mathbb{V}_d$  (the results are similar for  $\Sigma_d$  and  $\mathbb{W}_d$ )

$$[\mathbb{V}_d]_{11}(R_{\frac{2\pi}{3}}^* \mathbf{X}) = [\mathbb{V}_d]_{11}(\mathbf{X}), \quad [\mathbb{V}_d]_{12}(R_{\frac{2\pi}{3}}^* \mathbf{X}) = \omega [\mathbb{V}_d]_{12}(\mathbf{X}), \quad (45)$$

$$[\mathbb{V}_d]_{21}(R_{\frac{2\pi}{3}}^* \mathbf{X}) = \bar{\omega} [\mathbb{V}_d]_{21}(\mathbf{X}), \quad [\mathbb{V}_d]_{22}(R_{\frac{2\pi}{3}}^* \mathbf{X}) = [\mathbb{V}_d]_{22}(\mathbf{X}). \quad (46)$$

We now consider the  $\mathcal{CP}$  symmetry. Using the definition of  $\Phi_2$  in (6) we deduce that for  $\alpha \in L^2(\mathbb{R}^2; \mathbb{C}^4)$ ,

$$(\mathcal{CP})(\alpha : \Phi)_{d,\theta} = ((\mathcal{CP}\alpha) : (\mathcal{CP}\Phi))_{d,\theta} = \left( (\widetilde{\mathcal{CP}}\alpha) : \Phi \right)_{d,\theta},$$

where  $\widetilde{\mathcal{CP}}$  is the anti-unitary of  $L^2(\mathbb{R}^2; \mathbb{C}^4)$  defined by

$$\widetilde{\mathcal{CP}} \begin{pmatrix} \alpha_{+,1} \\ \alpha_{+,2} \\ \alpha_{-,1} \\ \alpha_{-,2} \end{pmatrix} = (\mathcal{CP}) \begin{pmatrix} \alpha_{+,2} \\ \alpha_{+,1} \\ \alpha_{-,2} \\ \alpha_{-,1} \end{pmatrix} = \begin{pmatrix} 0 & (\mathcal{CP}) & 0 & 0 \\ (\mathcal{CP}) & 0 & 0 & 0 \\ 0 & 0 & 0 & (\mathcal{CP}) \\ 0 & 0 & (\mathcal{CP}) & 0 \end{pmatrix} \begin{pmatrix} \alpha_{+,1} \\ \alpha_{+,2} \\ \alpha_{-,1} \\ \alpha_{-,2} \end{pmatrix}.$$

We deduce as previously that

$$\left[ \mathcal{S}_d, \widetilde{\mathcal{CP}} \right] = 0, \quad \text{and} \quad \left[ \mathcal{H}_{d,\theta}, \widetilde{\mathcal{CP}} \right] = 0,$$

from which we infer, for  $\mathbb{V}_d$  (the results are similar for  $\Sigma_d$  and  $\mathbb{W}_d^\pm$ )

$$\overline{[\mathbb{V}_d]_{11}(-\mathbf{X})} = [\mathbb{V}_d]_{22}(\mathbf{X}) \quad \text{and} \quad \overline{[\mathbb{V}_d]_{12}(-\mathbf{X})} = [\mathbb{V}_d]_{21}(\mathbf{X}). \quad (47)$$

Finally, we consider the mirror symmetry, coming from the  $\mathfrak{R}$  operator. Using the relation  $\mathfrak{R}\Phi_1 = -\Phi_2$ , we get

$$(\mathfrak{R})(\alpha : \Phi)_{d,\theta} = ((\mathfrak{R}\alpha) : (\mathfrak{R}\Phi))_{d,\theta} = \left( (\widetilde{\mathfrak{R}}\alpha) : \Phi \right)_{d,\theta},$$

with, setting  $(\mathcal{M}f)(\mathbf{x}) = f(M\mathbf{x})$  with  $M = \begin{pmatrix} 1 & 0 \\ 0 & -1 \end{pmatrix}$ ,

$$\tilde{\mathfrak{R}} \begin{pmatrix} \alpha_{+,1} \\ \alpha_{+,2} \\ \alpha_{-,1} \\ \alpha_{-,2} \end{pmatrix} = -\mathcal{M} \begin{pmatrix} \alpha_{-,2} \\ \alpha_{-,1} \\ \alpha_{+,2} \\ \alpha_{+,1} \end{pmatrix} = \begin{pmatrix} 0 & 0 & 0 & -\mathcal{M} \\ 0 & 0 & -\mathcal{M} & 0 \\ 0 & -\mathcal{M} & 0 & 0 \\ -\mathcal{M} & 0 & 0 & 0 \end{pmatrix} \begin{pmatrix} \alpha_{+,1} \\ \alpha_{+,2} \\ \alpha_{-,1} \\ \alpha_{-,2} \end{pmatrix}.$$

Note that this time, since  $\mathfrak{R}U_{d,\theta} = U_{d,\theta}^* \mathfrak{R}$ , the mirror symmetry exchanges the top and bottom layers. From the relations

$$[\mathcal{S}_d, \tilde{\mathfrak{R}}] = 0, \quad \text{and} \quad [\mathcal{H}_{d,\theta}, \tilde{\mathfrak{R}}] = 0,$$

we infer

$$\begin{aligned} [\mathbb{V}_d]_{11}(M\mathbf{X}) &= \overline{[\mathbb{V}_d]_{22}(\mathbf{X})}, & [\mathbb{V}_d]_{12}(M\mathbf{X}) &= \overline{[\mathbb{V}_d]_{12}(\mathbf{X})}, \\ [\mathbb{V}_d]_{21}(M\mathbf{X}) &= \overline{[\mathbb{V}_d]_{21}(\mathbf{X})}, & [\mathbb{V}_d]_{22}(M\mathbf{X}) &= \overline{[\mathbb{V}_d]_{22}(\mathbf{X})}, \end{aligned}$$

and similar relations for  $\Sigma_d$ , as well as

$$\begin{aligned} [\mathbb{W}^+]_{11}(M\mathbf{X}) &= [\mathbb{W}^-]_{22}(\mathbf{X}), & [\mathbb{W}^+]_{12}(M\mathbf{X}) &= [\mathbb{W}^-]_{21}(\mathbf{X}), \\ [\mathbb{W}^+]_{21}(M\mathbf{X}) &= [\mathbb{W}^-]_{12}(\mathbf{X}), & [\mathbb{W}^+]_{22}(M\mathbf{X}) &= [\mathbb{W}^-]_{11}(\mathbf{X}). \end{aligned}$$

### 3.3.3 Extra symmetries at the limit

In addition to the previously identified symmetries, extra symmetries appear due to the averaging process over all possible stacking. Indeed, we claim that

$$\mathcal{C}((f, g))_d^{\eta\eta'} = ((g, f))_d^{\eta'\eta}, \quad (48)$$

$$\mathcal{CP}((f, g))_d^{+-} = ((\mathcal{S}g, \mathcal{S}f))_d^{+-}, \quad (49)$$

$$((f, g))_d^{+-} = ((\mathcal{CP}g, \mathcal{CP}f))_d^{+-}. \quad (50)$$

Equality (48) comes directly from the definition (36). To prove the second equality, we write

$$\begin{aligned} \overline{((f, g))_d^{+-}(-\mathbf{X})} &= \int_{\Omega \times \mathbb{R}} f(\mathbf{x} + \tfrac{1}{2}J\mathbf{X}, z - \tfrac{d}{2}) \overline{g(\mathbf{x} - \tfrac{1}{2}J\mathbf{X}, z + \tfrac{d}{2})} \, d\mathbf{x} \, dz \\ &= \int_{\Omega \times \mathbb{R}} \overline{g(\mathbf{x} - \tfrac{1}{2}J\mathbf{X}, -z + \tfrac{d}{2})} f(\mathbf{x} + \tfrac{1}{2}J\mathbf{X}, -z - \tfrac{d}{2}) \, d\mathbf{x} \, dz \\ &= \int_{\Omega \times \mathbb{R}} \overline{\mathcal{S}g(\mathbf{x} - \tfrac{1}{2}J\mathbf{X}, z - \tfrac{d}{2})} \mathcal{S}f(\mathbf{x} + \tfrac{1}{2}J\mathbf{X}, z + \tfrac{d}{2}) \, d\mathbf{x} \, dz = ((\mathcal{S}g, \mathcal{S}f))_d^{+-}(\mathbf{X}). \end{aligned}$$

The relation (50) follows from similar arguments.

From (48), we deduce that

$$[\mathbb{W}_d^+]_{11}(\mathbf{X}) = [\mathbb{W}_d^-]_{22}(\mathbf{X}), \quad \text{and} \quad [\mathbb{W}_d^+]_{22}(\mathbf{X}) = [\mathbb{W}_d^-]_{11}(\mathbf{X}),$$

and all these quantities are real-valued. Next, from (49), we deduce that

$$\Sigma_d(-\mathbf{X})^* = \Sigma_d(\mathbf{X}), \quad \mathbb{V}_d(-\mathbf{X})^* = \mathbb{V}_d(\mathbf{X}), \quad \text{and} \quad \mathbb{W}_d^+(-\mathbf{X})^* = \mathbb{W}_d^-(\mathbf{X}).$$

Finally, from (50), we obtain that

$$[\Sigma_d]_{11}(\mathbf{X}) = [\Sigma_d]_{22}(\mathbf{X}), \quad [\mathbb{V}_d]_{11}(\mathbf{X}) = [\mathbb{V}_d]_{22}(\mathbf{X}), \quad [\mathbb{W}_d^+]_{12}(\mathbf{X}) = [\mathbb{W}_d^-]_{21}(\mathbf{X}).$$

### 3.3.4 Energy gauge

We remark that if we change the energy reference at the single-layer level, that is if we add a constant  $c \in \mathbb{R}$  to the single-layer potential  $V \rightarrow V + c$ , then  $V_{\text{int},d}$  does not change because it is a difference, but  $\mathbb{V}_d \rightarrow \mathbb{V}_d + c\Sigma_d$  and  $\mathbb{W}_d^\pm \rightarrow \mathbb{W}_d^\pm + c\mathbb{I}_2$  so  $\mathcal{H}_{d,\theta} \rightarrow \mathcal{H}_{d,\theta} + c\mathcal{S}_d$ , which only effect is to shift the energies of  $c$ .

## 3.4 Comparison with the Bistritzer-MacDonald model

The Bistritzer-MacDonald Hamiltonian (1) can be written more explicitly [6, 27] as

$$H_\theta^{\text{BM}} = \begin{pmatrix} v_F \boldsymbol{\sigma}_{\theta/2} \cdot (-i\nabla_{\mathbf{x}}) & V(\varepsilon_\theta \mathbf{x}) \\ V(\varepsilon_\theta \mathbf{x})^* & v_F \boldsymbol{\sigma}_{-\theta/2} \cdot (-i\nabla_{\mathbf{x}}) \end{pmatrix}, \quad (51)$$

with

$$\mathbf{V}(\mathbf{X}) := \begin{pmatrix} w_{\text{AA}} G(\mathbf{X}) & w_{\text{AB}} \overline{F(-\mathbf{X})} \\ w_{\text{AB}} F(\mathbf{X}) & w_{\text{AA}} G(\mathbf{X}) \end{pmatrix}, \quad (52)$$

where  $w_{\text{AA}}$  and  $w_{\text{AB}}$  are the two real parameters describing the interlayer coupling in AA and AB stacking, and

$$F(\mathbf{X}) := e^{-i\mathbf{q}_1 \cdot \mathbf{X}} + \omega e^{-i\mathbf{q}_2 \cdot \mathbf{X}} + \omega^2 e^{-i\mathbf{q}_3 \cdot \mathbf{X}}, \quad G(\mathbf{X}) := e^{-i\mathbf{q}_1 \cdot \mathbf{X}} + e^{-i\mathbf{q}_2 \cdot \mathbf{X}} + e^{-i\mathbf{q}_3 \cdot \mathbf{X}}. \quad (53)$$

We have for all  $\mathbf{R}_M = m_1 \mathbf{a}_{1,M} + m_2 \mathbf{a}_{2,M} \in \mathbb{L}_M$ ,

$$\begin{aligned} F(\mathbf{X} - \mathbf{R}_M) &= e^{i\mathbf{q}_1 \cdot \mathbf{R}_M} F(\mathbf{X}) = \omega^{2(m_1+m_2)} F(\mathbf{X}), \\ G(\mathbf{X} - \mathbf{R}_M) &= e^{i\mathbf{q}_1 \cdot \mathbf{R}_M} G(\mathbf{X}) = \omega^{2(m_1+m_2)} G(\mathbf{X}), \end{aligned}$$

hence

$$\mathbf{V}(\mathbf{X} - \mathbf{R}_M) = e^{i\mathbf{q}_1 \cdot \mathbf{R}_M} \mathbf{V}(\mathbf{X}) = \omega^{2(m_1+m_2)} \mathbf{V}(\mathbf{X}). \quad (54)$$

Since

$$R_{\frac{2\pi}{3}} \mathbf{q}_1 = \mathbf{q}_2, \quad R_{\frac{2\pi}{3}} \mathbf{q}_2 = \mathbf{q}_3, \quad R_{\frac{2\pi}{3}} \mathbf{q}_3 = \mathbf{q}_1, \quad (55)$$

and  $\omega^2 = \bar{\omega}$ , we also have

$$F(R_{\frac{2\pi}{3}}^* \mathbf{X}) = \bar{\omega} F(\mathbf{X}) \quad \text{and} \quad G(R_{\frac{2\pi}{3}}^* \mathbf{X}) = G(\mathbf{X}), \quad (56)$$

yielding

$$[\mathbf{V}]_{11}(R_{\frac{2\pi}{3}}^* \mathbf{X}) = [\mathbf{V}]_{11}(\mathbf{X}), \quad [\mathbf{V}]_{12}(R_{\frac{2\pi}{3}}^* \mathbf{X}) = \omega [\mathbf{V}]_{12}(\mathbf{X}), \quad (57)$$

$$[\mathbf{V}]_{21}(R_{\frac{2\pi}{3}}^* \mathbf{X}) = \bar{\omega} [\mathbf{V}]_{21}(\mathbf{X}), \quad [\mathbf{V}]_{22}(R_{\frac{2\pi}{3}}^* \mathbf{X}) = [\mathbf{V}]_{22}(\mathbf{X}). \quad (58)$$

Finally, using the fact that  $G(\mathbf{X}) = \overline{G(-\mathbf{X})}$ , we get

$$[\mathbf{V}]_{11}(\mathbf{X}) = \overline{[\mathbf{V}]_{22}(-\mathbf{X})} \quad \text{and} \quad [\mathbf{V}]_{12}(\mathbf{X}) = \overline{[\mathbf{V}]_{21}(-\mathbf{X})}. \quad (59)$$

Rescaling lengths and energies as  $\mathbf{X} = \varepsilon_\theta \mathbf{x}$  and  $\mathcal{E} = \varepsilon_\theta^{-1} E$  (in the BM model, the Fermi level is set to zero), we obtain the rescaled BM Hamiltonian

$$\mathcal{H}_\theta^{\text{BM}} = \begin{pmatrix} v_F \boldsymbol{\sigma}_{\theta/2} \cdot (-i\nabla_{\mathbf{x}}) & \varepsilon_\theta^{-1} \mathbf{V}(\mathbf{x}) \\ \varepsilon_\theta^{-1} \mathbf{V}(\mathbf{x})^* & v_F \boldsymbol{\sigma}_{-\theta/2} \cdot (-i\nabla_{\mathbf{x}}) \end{pmatrix} \quad (60)$$



Going back to our model, we see that our effective Hamiltonian can be written of the form

$$\begin{aligned}\mathcal{H}_{d,\theta} = & \begin{pmatrix} v_F \boldsymbol{\sigma}_{\theta/2} \cdot (-i\nabla_{\mathbf{X}}) & \varepsilon_{\theta}^{-1} \mathbb{V}_d(\mathbf{X}) \\ \varepsilon_{\theta}^{-1} \mathbb{V}_d(\mathbf{X})^* & v_F \boldsymbol{\sigma}_{-\theta/2} \cdot (-i\nabla_{\mathbf{X}}) \end{pmatrix} + \begin{pmatrix} \varepsilon_{\theta}^{-1} \mathbb{W}_d^+ & 0 \\ 0 & \varepsilon_{\theta}^{-1} \mathbb{W}_d^- \end{pmatrix} \\ & + \begin{pmatrix} 0 & c_{\theta} J(-i\nabla \Sigma_d(\mathbf{X})) \cdot (-i\nabla) \\ c_{\theta} J(-i\nabla \Sigma_d^*(\mathbf{X})) \cdot (-i\nabla) & 0 \end{pmatrix} \\ & - \frac{\varepsilon_{\theta}}{2} \operatorname{div} \left( \begin{pmatrix} 0 & \Sigma_d(\mathbf{X}) \\ \Sigma_d^*(\mathbf{X}) & 0 \end{pmatrix} \nabla \bullet \right) - \frac{\varepsilon_{\theta}}{2} \Delta\end{aligned}$$

We see that the two models are similar under the following assumptions (which will be justified numerically in Section 4):

1. the matrix  $\Sigma_d(\mathbf{X})$  and its gradient can be neglected;
2. the term  $-\frac{1}{2}\varepsilon_{\theta}\Delta$  can be neglected, which is the case if the oscillations of the envelope functions  $\alpha_{\eta,j}$  at the moiré scale contribute more than those at the atomic scale;
3. the functions  $\mathbb{W}_d^{\pm}$  are almost proportional to the identity matrix (and thus only induce a global energy shift);
4. the function  $\mathbb{V}_d$  is almost of the form (52) for some well-chosen parameters  $w_{AA}$  and  $w_{AB}$ .

As for the last point, let us note that the functions  $\mathbb{V}_d$  and  $\mathbf{V}$  have the same quasi-periodicity properties (see (44) and (54)), and transform similarly under  $\frac{2\pi}{3}$ -rotation (see (45)-(46) and (57)-(58)) and  $\mathcal{CP}$ -symmetry (see (47) and (59)). First-principle values of the BM parameters can be inferred by relying on the fact that  $\mathbb{V}_d$  is exactly of the form (52) if and only if the interlayer coupling parameters are given by

$$w_{AA}^d := \frac{1}{3|\Omega_M|} \int_{\Omega_M} [\mathbb{V}_d]_{11}(\mathbf{X}) \overline{G(\mathbf{X})} d\mathbf{X}, \quad (61)$$

$$w_{AB}^d := \frac{1}{3|\Omega_M|} \int_{\Omega_M} [\mathbb{V}_d]_{21}(\mathbf{X}) \overline{F(\mathbf{X})} d\mathbf{X}, \quad (62)$$

where we used the fact that  $\int_{\Omega_M} |F|^2 = \int_{\Omega_M} |G|^2 = 3|\Omega_M|$ . Note that the integrands in (61) and (62) are  $\mathbb{L}_M$ -periodic functions, and that  $|\Omega_M| = |\Omega| = \frac{\sqrt{3}}{2}a_0^2$ . Let us now prove that

$$w_{AA}^d = w_{AB}^d \in \mathbb{R}. \quad (63)$$

First, we deduce from (34), (43), (53), (55), and (57) that

$$\begin{aligned}w_{AA}^d &= \frac{1}{3|\Omega_M|} \left( \sum_{n=1}^3 \int_{\Omega_M} [\mathbb{V}_d]_{11}(\mathbf{X}) e^{i\mathbf{q}_n \cdot \mathbf{X}} d\mathbf{X} \right) \\ &= \frac{1}{3|\Omega_M|} \left( \sum_{n=1}^3 \int_{\Omega_M} [\mathbb{V}_d]_{11} \left( R_{\frac{4\pi}{3}(n-1)}^* \mathbf{X} \right) e^{i\mathbf{q}_n \cdot \left( R_{\frac{4\pi}{3}(n-1)}^* \mathbf{X} \right)} d\mathbf{X} \right) \\ &= \frac{1}{3|\Omega_M|} \left( \sum_{n=1}^3 \int_{\Omega_M} [\mathbb{V}_d]_{11}(\mathbf{X}) e^{i \left( R_{\frac{4\pi}{3}(n-1)} \mathbf{q}_n \right) \cdot \mathbf{X}} d\mathbf{X} \right) \\ &= \frac{1}{3|\Omega_M|} \left( \sum_{n=1}^3 \int_{\Omega_M} [\mathbb{V}_d]_{11}(\mathbf{X}) e^{i\mathbf{q}_1 \cdot \mathbf{X}} d\mathbf{X} \right) \\ &= \frac{1}{|\Omega_M|} \int_{\Omega_M} ((V + V_{\text{int},d}(\cdot + \frac{d}{2})) u_1, u_1)_d^{+-}(\mathbf{X}) d\mathbf{X}.\end{aligned}$$

Using the definition (36) of  $((f, g))_d^{+-}(\mathbf{X})$  and after some change of variables in the integrals, we get

$$w_{AA}^d = \frac{1}{|\Omega|} \int_{\mathbb{R}} \left( \int_{\Omega} \overline{[(V + V_{\text{int},d}(\cdot + \frac{d}{2})) u_1]}(\mathbf{x}, z - \frac{d}{2}) d\mathbf{x} \right) \left( \int_{\Omega} u_1(\mathbf{x}, z + \frac{d}{2}) d\mathbf{x} \right) dz. \quad (64)$$

Since  $\overline{u_1(x_1, x_2, z)} = u_1(-x_1, x_2, z)$ ,  $V$  and  $V_{\text{int}}$  are real-valued, and  $V(x_1, x_2, z) = V(-x_1, x_2, z)$ , the parameter  $w_{AA}^d$  is a real number. A similar calculation based on (34), (36), (43), (53), (55), and (58) leads to

$$w_{AB}^d = \frac{1}{|\Omega|} \int_{\mathbb{R}} \left( \int_{\Omega} \overline{[(V + V_{\text{int},d}(\cdot + \frac{d}{2})) u_2]}(\mathbf{x}, z - \frac{d}{2}) d\mathbf{x} \right) \left( \int_{\Omega} u_1(\mathbf{x}, z + \frac{d}{2}) d\mathbf{x} \right) dz,$$

and we conclude from (11) and the relations  $V(x_1, -x_2, z) = V(x_1, x_2, z)$  and  $u_2(x_1, -x_2, z) = u_2(x_1, x_2, z)$  that  $w_{AA}^d = w_{AB}^d$ .

The practical computation of  $w_{AA}^d = w_{AB}^d$  will be discussed in the next section.

## 4 Numerical results

In this section, we numerically study the generalized spectral problem associated to with the operators  $(\mathcal{H}_{d,\theta}, \mathcal{S}_d)$  defined in (31). First, we show in Section 4.1 that this problem is unitary equivalent to a generalized spectral problem involving  $\mathbb{L}_M$ -periodic operators  $(\tilde{\mathcal{H}}_{d,\theta}, \tilde{\mathcal{S}}_d)$  obtained by gauge transformation. Next, we study the Bloch band diagram of this moiré-periodic model. This gives eigenvalue equations of the form

$$\boxed{\tilde{\mathcal{H}}_{d,\theta,\mathbf{k}} \tilde{\alpha}_{n,\mathbf{k}} = \mathcal{E}_{d,\theta,n,\mathbf{k}} \tilde{\mathcal{S}}_d \tilde{\alpha}_{n,\mathbf{k}}}$$

where it is sufficient to consider the quasimomenta  $\mathbf{k}$  belonging to the first Brillouin zone  $\Omega_M^*$  of the moiré lattice (the set  $\varepsilon_\theta \Omega_M^*$  is often called the mini Brillouin zone). Due to the energy shift in (26) and the rescaling by  $\varepsilon_\theta$ , the spectrum of the operator  $H_{d,\theta}^{(2)}$  close to  $\mu_F$  is related to the spectra of  $(\mathcal{H}_{d,\theta}, \mathcal{S}_d)$  and  $(\tilde{\mathcal{H}}_{d,\theta}, \tilde{\mathcal{S}}_d)$  around 0 by

$$\sigma(H_{d,\theta}^{(2)}) \simeq \mu_F + \varepsilon_\theta \sigma(\mathcal{H}_{d,\theta}, \mathcal{S}_d) = \mu_F + \varepsilon_\theta \sigma(\tilde{\mathcal{H}}_{d,\theta}, \tilde{\mathcal{S}}_d).$$

### 4.1 Gauge transformation

First, we perform a gauge transformation in order to remove the phase factors in (44) and end up with an  $\mathbb{L}_M$ -periodic model. The same arguments can be used for the BM model. Let  $\mathbf{K}_1$  and  $\mathbf{K}_2$  be two vectors such that  $\mathbf{K}_1 - \mathbf{K}_2 = \mathbf{q}_1$ . One can choose for instance  $\mathbf{K}_2 = \mathbf{q}_3 = \frac{1}{3}(-\mathbf{a}_{1,M}^* + 2\mathbf{a}_{2,M}^*)$ , and  $\mathbf{K}_1 = -\mathbf{q}_2 = \frac{1}{3}(-2\mathbf{a}_{1,M}^* + \mathbf{a}_{2,M}^*)$  (recall that  $\mathbf{q}_1 + \mathbf{q}_2 + \mathbf{q}_3 = \mathbf{0}$ ), but another choice is possible. We introduce the unitary multiplication operator

$$P(\mathbf{X}) := \begin{pmatrix} e^{i\mathbf{K}_1 \cdot \mathbf{X}} \mathbb{I}_2 & \mathbf{0} \\ \mathbf{0} & e^{i\mathbf{K}_2 \cdot \mathbf{X}} \mathbb{I}_2 \end{pmatrix}, \quad \text{with inverse} \quad P^*(\mathbf{X}) := \begin{pmatrix} e^{-i\mathbf{K}_1 \cdot \mathbf{X}} \mathbb{I}_2 & 0 \\ 0 & e^{-i\mathbf{K}_2 \cdot \mathbf{X}} \mathbb{I}_2 \end{pmatrix}.$$

First, we have

$$\tilde{\mathcal{S}}_d := P \mathcal{S}_d P^* = \begin{pmatrix} \mathbb{I}_2 & \tilde{\Sigma}_d(\mathbf{X}) \\ \tilde{\Sigma}_d^*(\mathbf{X}) & \mathbb{I}_2 \end{pmatrix},$$

with, using (33) and the fact that  $\mathbf{q}_1 = J\mathbf{K}$ ,

$$\tilde{\Sigma}_d(\mathbf{X}) = e^{i(\mathbf{K}_1 - \mathbf{K}_2) \cdot \mathbf{X}} \Sigma_d(\mathbf{X}) = e^{i\mathbf{q}_1 \cdot \mathbf{X}} \Sigma_d(\mathbf{X}) = ((u_j, u_{j'}))_d^{+-}(\mathbf{X}).$$

The  $\widetilde{\mathcal{S}}_d$  matrix-valued function is now  $\mathbb{L}_M$ -periodic. Similarly, the operator

$$\widetilde{\mathcal{H}}_{d,\theta} := P\mathcal{H}_{d,\theta}P^* = \varepsilon_\theta^{-1}\widetilde{\mathcal{V}}_d + c_\theta\widetilde{T}_d + \varepsilon_\theta\widetilde{T}_d^{(1)}.$$

is  $\mathbb{L}_M$ -periodic with components given by

$$\widetilde{\mathcal{V}}_d = \begin{pmatrix} \widetilde{\mathbb{W}}_d^+(\mathbf{X}) & \widetilde{\mathbb{V}}_d(\mathbf{X}) \\ \widetilde{\mathbb{V}}_d(\mathbf{X})^* & \widetilde{\mathbb{W}}_d^-(\mathbf{X}) \end{pmatrix},$$

$$\widetilde{T}_d = \begin{pmatrix} v_F\boldsymbol{\sigma} \cdot (-i\nabla - \mathbf{K}_1) & J\widetilde{A}_d(\mathbf{X}) \cdot (-i\nabla - \mathbf{K}_2) \\ J(\widetilde{A}_d)^*(\mathbf{X}) \cdot (-i\nabla - \mathbf{K}_1) & v_F\boldsymbol{\sigma} \cdot (-i\nabla - \mathbf{K}_2) \end{pmatrix},$$

where  $\widetilde{A}_d := -i\nabla\Sigma_d = (-i\nabla - \mathbf{q}_1)\widetilde{\Sigma}_d$ , and

$$\widetilde{T}_d^{(1)} = \frac{1}{2} \begin{pmatrix} (-i\nabla - \mathbf{K}_1)^2 - v_F\boldsymbol{\sigma} \cdot J(-i\nabla - \mathbf{K}_1) & (-i\nabla - \mathbf{K}_1) \cdot [\widetilde{\Sigma}_d(-i\nabla - \mathbf{K}_2)\bullet] \\ (-i\nabla - \mathbf{K}_2) \cdot [\widetilde{\Sigma}_d^*(-i\nabla - \mathbf{K}_1)\bullet] & (-i\nabla - \mathbf{K}_2)^2 + v_F\boldsymbol{\sigma} \cdot J(-i\nabla - \mathbf{K}_2) \end{pmatrix},$$

with

$$[\widetilde{\Sigma}_d(\mathbf{X})]_{jj'} := ((u_j, u_{j'}))_d^{+-}(\mathbf{X}), \quad (65)$$

$$[\widetilde{\mathbb{V}}_d(\mathbf{X})]_{jj'} := (((V + V_{\text{int},d}(\cdot + \frac{d}{2}))u_j, u_{j'}))_d^{+-}(\mathbf{X}), \quad (66)$$

$$[\widetilde{\mathbb{W}}_d^\pm(\mathbf{X})]_{jj'} := ((u_j\overline{u_{j'}}, V))_d^{\pm\mp}(\mathbf{X}) + (W_{\text{int},d}^\pm)_{jj'}. \quad (67)$$

In this gauge, the model is  $\mathbb{L}_M$  periodic, and we can apply the usual Bloch transform to compute its band diagram. For the sake of illustration, we display on Fig. 10 the band diagrams of the BM model (black) and of our continuous model (red) for the first minimal bandwidth angles (resp.  $\theta \simeq 1.174^\circ$  and  $\theta \simeq 1.155^\circ$ ). A thorough comparison of the band diagrams of various continuous models (including atomic relaxation) will be the matter of a forthcoming paper.

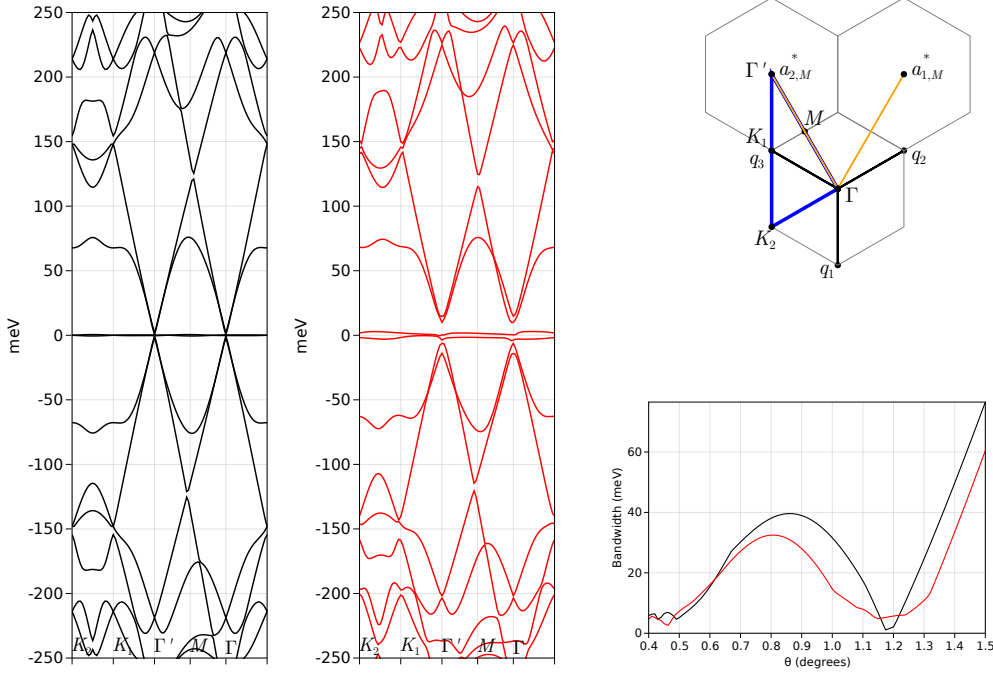


Figure 4: Quantities are computed with  $d = 6.45$  bohr for our effective model, and  $w_{AA} = w_{AB} = 110$  meV for  $\mathcal{H}_\theta^{\text{BM}}$ . Top right: path  $\mathbf{K}_2 \rightarrow \mathbf{K}_1 \rightarrow \Gamma' \rightarrow M \rightarrow \Gamma \rightarrow \mathbf{K}_2$  of the band diagrams. Bottom right: bandwidths of the Fermi bands over the previous path, of  $\mathcal{H}_\theta^{\text{BM}}$  (black) having  $w_{AA} = w_{AB} = 110$  meV, and of  $(\tilde{\mathcal{H}}_{d,\theta}, \tilde{\mathcal{S}}_d)$  (red) against  $\theta$ . (Left) band diagram of  $\mathcal{H}_\theta^{\text{BM}}$  (black) for the first minimal bandwidth angle  $\theta \simeq 1.174^\circ$  (bandwidth 1.1 meV), band diagram of  $(\tilde{\mathcal{H}}_{d,\theta}, \tilde{\mathcal{S}}_d)$  (red) for the first minimal bandwidth angle  $\theta \simeq 1.155^\circ$  (bandwidth 1.5 meV).

## 4.2 Computation of the parameters of the reduced model

We now explain how to numerically compute the fields  $\widetilde{\Sigma}_d(\mathbf{X})$ ,  $\widetilde{\mathbb{V}}_d(\mathbf{X})$  and  $\widetilde{\mathbb{W}}_d^\pm(\mathbf{X})$  as well as the ‘optimal’ BM parameters  $w_{AA}^d = w_{AB}^d$  defined in (61)-(62). We also compare our reduced model to the original BM model parameterized with the so-computed values of interlayer coupling. The technicalities introduced by the nonlocal component of the pseudopotential are addressed in Appendix B.

In view of (65)-(67), it suffices to detail the practical computation of  $((f, g))_d^\pm(\mathbf{X})$  for  $f, g \in L_{\text{per}}^2$ , as well as that of the integrals in (37). In standard plane-wave numerical simulations, the infinite domain  $\Omega \times \mathbb{R}$  is replaced by the finite domain  $\Omega \times (-L_z/2, L_z/2)$  with  $L_z$  large enough, and the considered functions in  $\Omega \times (-L_z/2, L_z/2)$  are assumed to satisfy either periodic or homogeneous Dirichlet boundary conditions in the transverse direction. As a consequence, the functions  $u_j$ ,  $Vu_j$ , and  $u_j \overline{u_j'}$  can be expanded in Fourier series as

$$f(\mathbf{r}) = \sum_{m_1, m_2, m_z \in \mathbb{Z}} [f]_{m_1, m_2, m_z} \frac{e^{i((m_1 \mathbf{a}_1^* + m_2 \mathbf{a}_2^*) \cdot \mathbf{x} + m_z \frac{2\pi z}{L_z})}}{|\Omega|^{1/2} L_z^{1/2}} \quad (f = u_j, Vu_j, \text{ or } u_j \overline{u_j'}), \quad (68)$$

and the function  $V_{\text{int},d}$  as

$$V_{\text{int},d}(z) := \sum_{m_z \in \mathbb{Z}} [V_{\text{int},d}]_{m_z} \frac{e^{im_z \frac{2\pi z}{L_z}}}{L_z^{1/2}}.$$

For  $f$  and  $g$  of the form (68), we have (with a slight abuse of notation)

$$\begin{aligned} ((f, g))_d^{+-}(\mathbf{X}) &:= \int_{\Omega \times [-L_z/2, L_z/2]} \overline{f(\mathbf{x} - \frac{1}{2}J\mathbf{X}, z - \frac{d}{2})} g(\mathbf{x} + \frac{1}{2}J\mathbf{X}, z + \frac{d}{2}) d\mathbf{x} dz \\ &= \sum_{m_1, m_2, m_z \in \mathbb{Z}} [\overline{f}]_{m_1, m_2, m_z} [g]_{m_1, m_2, m_z} e^{i(m_1 \mathbf{a}_1^* + m_2 \mathbf{a}_2^*) \cdot J\mathbf{X}} e^{im_z \frac{2\pi}{L_z} d}. \end{aligned}$$

Since  $\mathbf{a}_{1,M}^* = J\mathbf{a}_1^*$  and  $\mathbf{a}_{2,M}^* = J\mathbf{a}_2^*$ , we deduce that we have

$$((f, g))_d^{+-}(\mathbf{X}) = \sum_{m_1, m_2 \in \mathbb{Z}} [f|g]_{d, m_1, m_2} \frac{e^{i(m_1 \mathbf{a}_{1,M}^* + m_2 \mathbf{a}_{2,M}^*) \cdot \mathbf{X}}}{|\Omega_M|^{1/2}}$$

with

$$[f|g]_{d, m_1, m_2} := |\Omega_M|^{1/2} \sum_{m_z \in \mathbb{Z}} [\overline{f}]_{-m_1, -m_2, m_z} [g]_{-m_1, -m_2, m_z} e^{im_z \frac{2\pi}{L_z} d}. \quad (69)$$

This formula is in agreement with the fact that  $((f, g))_d^{+-}(\mathbf{X})$  can be written as a convolution operator, see (38). Similarly, the scalars  $(W_{\text{int}, d}^\pm)_{jj'}$  in (37) are given by

$$(W_{\text{int}, d}^\pm)_{jj'} = |\Omega_M|^{1/2} \sum_{m_z \in \mathbb{Z}} [\overline{u_j u_{j'}}]_{0, 0, m_z} [V_{\text{int}, d}]_{m_z} e^{\pm im_z \frac{2\pi}{L_z} d}. \quad (70)$$

In order to numerically compute the Fourier coefficients of  $[\widetilde{\Sigma}_d]_{jj'}$ ,  $[\widetilde{\mathbb{V}}_d]_{jj'}$ , and  $[\widetilde{\mathbb{W}}_d^\pm]_{jj'}$ , we have developed a code in Julia [4], interfaced with the DFTK planewave DFT package [17].

The single-layer graphene Kohn-Sham model is solved with DFTK using the PBE exchange-correlation functional with Goedecker-Teter-Hutter (GTH) pseudopotential, a unit cell of height  $L_z = 110$  bohr, an energy cut-off of  $E_{\text{cut}} = 900$  eV, and a  $(5 \times 5 \times 1)$   $k$ -point grid. We extract from the DFTK computation  $\mathbb{L}$ -periodic functions  $u_1$  and  $u_2$  such that  $\Phi_1(\mathbf{r}) = e^{i\mathbf{K} \cdot \mathbf{r}} u_1(\mathbf{r})$  and  $\Phi_2(\mathbf{r}) = e^{i\mathbf{K} \cdot \mathbf{r}} u_2(\mathbf{r})$  form an orthogonal basis of  $\text{Ker} \left( H_{\mathbf{K}}^{(1)} - \mu_F \right)$ , where  $H_{\mathbf{K}}^{(1)}$  is the Bloch fiber of the single-layer graphene Kohn-Sham Hamiltonian at the Dirac point  $\mathbf{K}$ . We also extract the local component of the single-layer graphene Kohn-Sham potential  $V$  (as well as the required information on the nonlocal component of the carbon atom GTH pseudopotential, see Appendix B for details). More precisely, DFTK returns the Fourier coefficients of the  $\mathbb{L}$ -periodic functions  $u_j$ ,  $V$ : at the discrete level, the sums in (68) are finite and run over the triplets of integers  $(m_1, m_2, m_z) \in \mathbb{Z}^3$  such that

$$\frac{|m_1 \mathbf{a}_1^* + m_2 \mathbf{a}_2^* + \mathbf{K}|^2 + m_z^2 \frac{4\pi^2}{L_z^2}}{2} \leq E_{\text{cut}}.$$

We then replace  $u_1$  and  $u_2$  by the unique linear combination of these functions such that (9), (11) and (12) are satisfied, and transform the Fourier coefficients in (68) accordingly. In the expressions below, the Fourier coefficients are those obtained *after* this transformation.

The Kohn-Sham potential  $V_{d, \mathbf{y}}^{(2)}$  is computed for each disregistry  $\mathbf{y}$  in a  $(5 \times 5)$  uniform grid of the graphene unit cell, and the function  $V_{\text{int}, d}(z)$  is obtained using (15)-(16). In the results reported below, we used the experimental interlayer mean distance  $d = 6.45$  bohr. In accordance with the results in [28], the potential  $V_{\text{int}, d, \mathbf{y}}(z)$  only slightly depends on  $\mathbf{y}$ :

$$\delta V_{\text{int}, d} := \frac{\int_{\Omega \times \mathbb{R}} |V_{\text{int}, d, \mathbf{y}}(z) - V_{\text{int}, d}(z)|^2 d\mathbf{y} dz}{|\Omega| \int_{\mathbb{R}} V_{\text{int}}(z)^2 dz} \simeq 1 \times 10^{-4}.$$

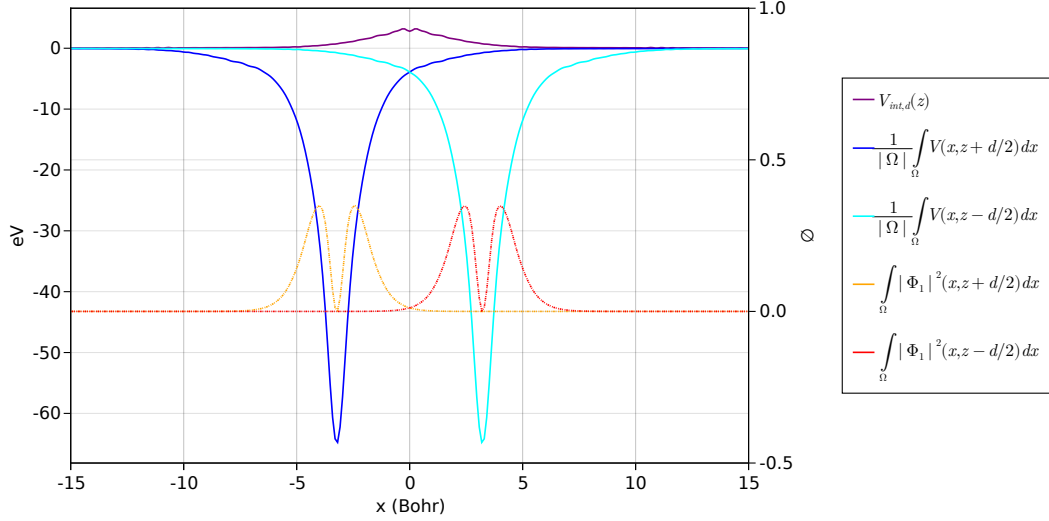


Figure 5: Effective potential  $V_{\text{int},d}$ , and in-plane averages of the vertically shifted single-layer Kohn-Sham potential  $V$  and Bloch wave densities  $|\Phi_1|^2$  for interlayer distance  $d = 6.45$  bohr.

The effective potential  $V_{\text{int},d}$ , and in-plane averages of the vertically shifted single-layer Kohn-Sham potential  $V$  and Bloch wave densities  $|\Phi_1|^2$  are plotted in Fig. 5.

From (63) and (64), we obtain

$$w_{\text{AA}}^d = w_{\text{AB}}^d = [V_d u_1 | u_1]_{d,0,0} \quad \text{where} \quad V_d := V + V_{d,\text{int}}(\cdot + \frac{d}{2}).$$

The ‘optimal’ value of the BM parameter can therefore be easily computed from the Fourier coefficients of  $u_1$ ,  $V u_1$ , and  $V_d$  using (69). For  $d = 6.45$  bohr, we obtain numerically

$$w_{\text{AA}}^{d=6.45 \text{ a.u.}} = w_{\text{BB}}^{d=6.45 \text{ a.u.}} \simeq 126 \text{ meV},$$

in good agreement with the value  $w_{\text{AA}} = w_{\text{AB}} = 110$  meV chosen in [6] to fit experimental data.

### 4.3 Numerical justification of the Bistritzer-MacDonald model

As discussed in Section 3.4, the BM model can be deduced from our reduced model by assuming that  $\Sigma_d(\mathbf{X})$  and its gradient can be neglected, that  $\mathbb{W}_d^\pm(\mathbf{X})$  is proportional to the identity matrix, and that  $\mathbb{V}_d(\mathbf{X})$  is of the form (52) for some well-chosen parameters  $w_{\text{AA}}$  and  $w_{\text{AB}}$ . To test these assumptions, we first plot in Figs. 6-9 the real-space structures and magnitudes of the functions  $[\Sigma_d]_{jj'}(\mathbf{X})$ ,  $|\nabla \Sigma_d(\mathbf{X})|$ ,  $[\mathbb{W}_d^\pm]_{jj'}(\mathbf{X}) - f_\Omega [\mathbb{W}_d^\pm]_{jj'}$  and  $[\mathbb{V}_d]_{jj'}(\mathbf{X}) - \mathbf{V}_{jj'}(\mathbf{X})$  for  $d = 6.45$  bohr and  $w_{\text{AA}} = w_{\text{BB}} = 126$  meV. We can see these fields are indeed small in the relevant units:  $\Sigma_d(\mathbf{X})$  is small ( $\sim 0.03$  compared to 1),  $|\nabla \Sigma_d(\mathbf{X})|$  is small ( $\sim 0.03$  compared to the Fermi velocity  $v_F \simeq 0.380$ ), and  $\mathbb{V}_d(\mathbf{X}) - \mathbf{V}(\mathbf{X})$  and  $\mathbb{W}_d^\pm(\mathbf{X}) - f_\Omega \mathbb{W}_d^\pm$  are small (resp.  $\sim 1$  meV and  $\sim 40$  meV compared to the interlayer characteristic interaction energy 126 meV). This provides a new argument supporting the validity of the BM model.

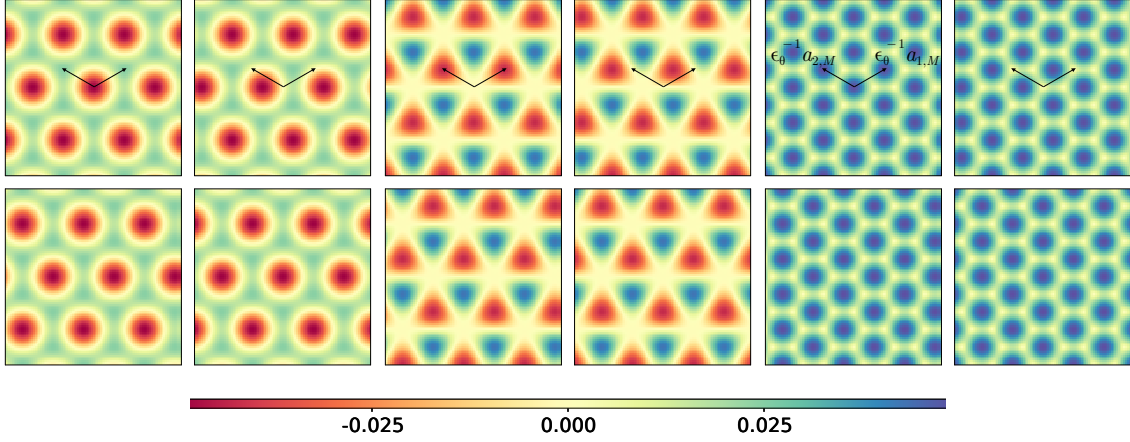


Figure 6: The 4 entries of resp. the real part, the imaginary part, and the modulus of the matrix-valued function  $\Sigma_d(\mathbf{X})$  for  $d = 6.45$  bohr.

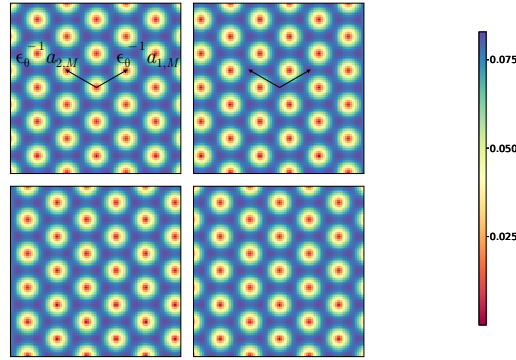


Figure 7: The 4 entries of the matrix-valued function  $|\nabla \Sigma_d(\mathbf{X})|/v_F$  for  $d = 6.45$  bohr.

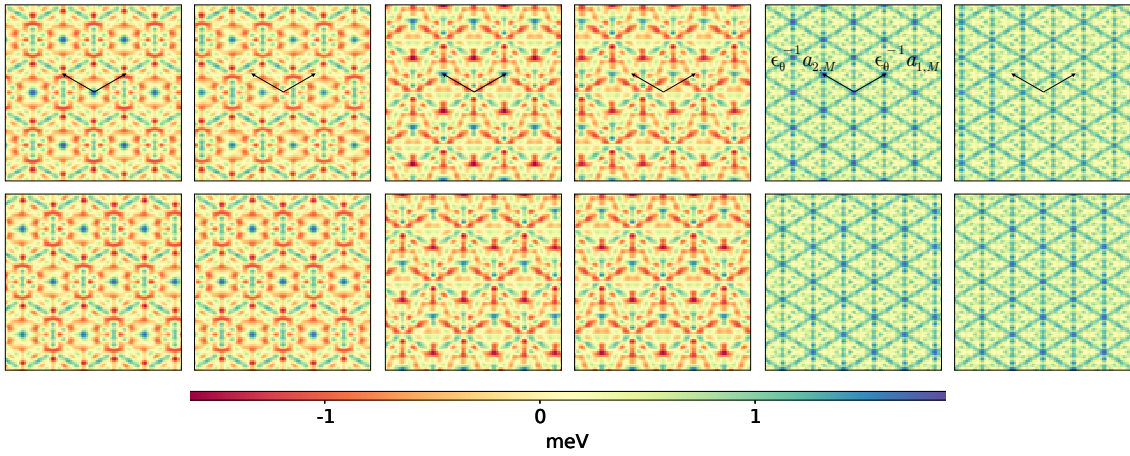


Figure 8: The 4 entries of resp. the real part, the imaginary part, and the modulus of the matrix-valued function  $V_d(\mathbf{X}) - V(\mathbf{X})$  for  $d = 6.45$  bohr and  $w_{AA} = w_{BB} = 126$  meV.

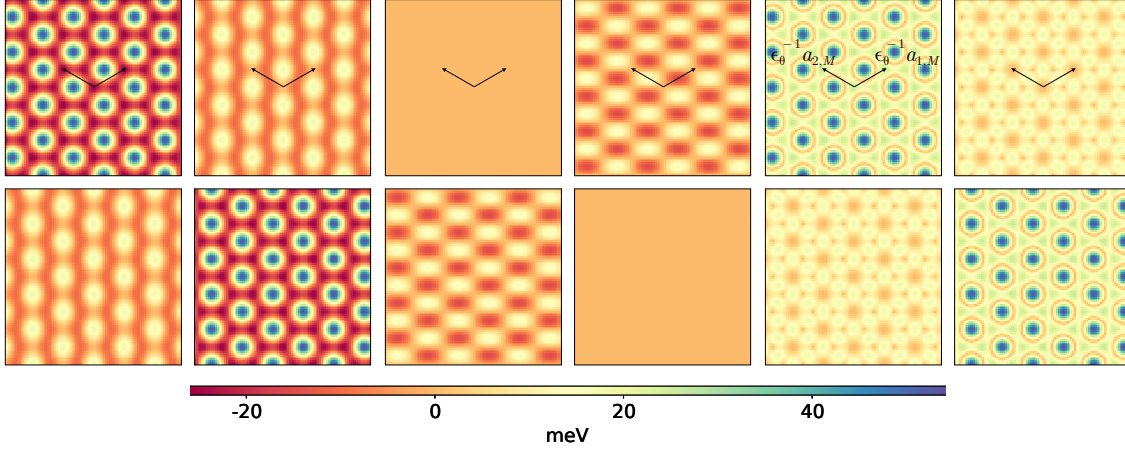


Figure 9: The 4 entries of resp. the real part, the imaginary part, and the modulus of the matrix-valued function  $\mathbb{W}_d^+(\mathbf{X}) - f_\Omega \mathbb{W}_d^+$  for  $d = 6.45$  bohr.

Let us finally study the variations of the fields  $\Sigma_d(\mathbf{X})$ ,  $\mathbb{V}_d(\mathbf{X})$  and  $\mathbb{W}_d^\pm(\mathbf{X})$  as functions of  $d$ . For  $A = (A_{ij})_{1 \leq i, j \leq 2} \in L^2(\Omega_M; \mathbb{C}^{2 \times 2})$ , we set

$$\|A\|_{L^2} := \left( \sum_{1 \leq i, j \leq 2} \|A_{ij}\|_{L^2(\Omega_M)}^2 \right)^{1/2}.$$

Let us expand the three fields of interest as

$$\Sigma_d(\mathbf{X}) = [u_1|u_1]_{d,0,0} \mathbf{S}^{(0)}(\mathbf{X}) + r_{\Sigma,d}(\mathbf{X}), \quad (71)$$

$$\mathbb{V}_d(\mathbf{X}) = w_{AA} \mathbf{S}^{(0)}(\mathbf{X}) + [V_d u_1|u_1]_{d,-1,-1} \mathbf{S}^{(1)}(\mathbf{X}) + r_{\mathbb{V},d}(\mathbf{X}), \quad (72)$$

$$\mathbb{W}_d^+(\mathbf{X}) = W_{\text{int},d}^+ \mathbb{I}_2 + \mathbf{W}_d^+(\mathbf{X}) + r_{\mathbb{W},d}(\mathbf{X}), \quad (73)$$

where  $[u_1|u_1]_{d,0,0}$ ,  $w_{AA} = [V_d u_1|u_1]_{d,0,0}$ ,  $[V_d u_1|u_1]_{d,-1,-1}$ , and  $W_{\text{int},d}^+$  are real numbers, and where

$$\mathbf{S}^{(0)}(\mathbf{X}) := \begin{pmatrix} G(\mathbf{X}) & \overline{F(-\mathbf{X})} \\ F(\mathbf{X}) & G(\mathbf{X}) \end{pmatrix}, \quad \mathbf{S}^{(1)}(\mathbf{X}) := \begin{pmatrix} G^{(1)}(\mathbf{X}) & \overline{F^{(1)}(-\mathbf{X})} \\ F^{(1)}(\mathbf{X}) & G^{(1)}(\mathbf{X}) \end{pmatrix},$$

$$\mathbf{W}_d^+(\mathbf{X}) := \begin{pmatrix} |[u_1|^2|V_d]_{d,0,1}| D(\mathbf{X}) & |[\overline{u_1} u_2|V_d]_{d,0,1}| \overline{Z(-\mathbf{X})} \\ |[\overline{u_1} u_2|V_d]_{d,0,1}| Z(\mathbf{X}) & |[u_1|^2|V_d]_{d,0,1}| D(\mathbf{X}) \end{pmatrix},$$



with

$$\begin{aligned}
G^{(1)}(\mathbf{X}) &:= e^{-i\mathbf{q}_1 \cdot \mathbf{X}} \left( e^{i(\mathbf{a}_1^* - \mathbf{a}_2^*) \cdot \mathbf{X}} + e^{i(\mathbf{a}_2^* - \mathbf{a}_1^*) \cdot \mathbf{X}} + e^{-i(\mathbf{a}_1^* + \mathbf{a}_2^*) \cdot \mathbf{X}} \right) \\
&= e^{i2\mathbf{q}_1 \cdot \mathbf{X}} + e^{i2\mathbf{q}_2 \cdot \mathbf{X}} + e^{i2\mathbf{q}_3 \cdot \mathbf{X}}, \\
F^{(1)}(\mathbf{X}) &:= e^{-i\mathbf{q}_1 \cdot \mathbf{X}} \left( \omega e^{i(\mathbf{a}_1^* - \mathbf{a}_2^*) \cdot \mathbf{X}} + \omega^2 e^{i(\mathbf{a}_2^* - \mathbf{a}_1^*) \cdot \mathbf{X}} + e^{-i(\mathbf{a}_1^* + \mathbf{a}_2^*) \cdot \mathbf{X}} \right) \\
&= e^{i2\mathbf{q}_1 \cdot \mathbf{X}} + \omega e^{i2\mathbf{q}_2 \cdot \mathbf{X}} + \omega^2 e^{i2\mathbf{q}_3 \cdot \mathbf{X}}, \\
D(\mathbf{X}) &:= \omega \left( e^{-i\mathbf{a}_2^* \cdot \mathbf{X}} + e^{i\mathbf{a}_1^* \cdot \mathbf{X}} + e^{i(-\mathbf{a}_1^* + \mathbf{a}_2^*) \cdot \mathbf{X}} \right) + \omega^2 \left( e^{-i\mathbf{a}_1^* \cdot \mathbf{X}} + e^{i\mathbf{a}_2^* \cdot \mathbf{X}} + e^{i(\mathbf{a}_1^* - \mathbf{a}_2^*) \cdot \mathbf{X}} \right) \\
&= \omega \left( e^{i(\mathbf{q}_1 - \mathbf{q}_3) \cdot \mathbf{X}} + e^{i(\mathbf{q}_2 - \mathbf{q}_1) \cdot \mathbf{X}} + e^{i(\mathbf{q}_3 - \mathbf{q}_2) \cdot \mathbf{X}} \right) + \text{c.c.}, \\
Z(\mathbf{X}) &:= \omega \left( e^{i\mathbf{a}_2^* \cdot \mathbf{X}} + e^{-i\mathbf{a}_2^* \cdot \mathbf{X}} \right) + \omega^2 \left( e^{i\mathbf{a}_1^* \cdot \mathbf{X}} + e^{-i\mathbf{a}_1^* \cdot \mathbf{X}} \right) + e^{i(\mathbf{a}_1^* - \mathbf{a}_2^*) \cdot \mathbf{X}} + e^{i(-\mathbf{a}_1^* + \mathbf{a}_2^*) \cdot \mathbf{X}} \\
&= 2 \left( \cos((\mathbf{q}_3 - \mathbf{q}_2) \cdot \mathbf{X}) + \omega \cos((\mathbf{q}_3 - \mathbf{q}_1) \cdot \mathbf{X}) + \omega^2 \cos((\mathbf{q}_2 - \mathbf{q}_1) \cdot \mathbf{X}) \right).
\end{aligned}$$

Note that the above four functions are expanded on the subdominant Fourier modes and fulfill the expected symmetry properties.

We infer from the data in Figure 10 that for all values of  $d$  around the experimental average interlayer distance  $d \simeq 6.45$  bohr, we have

$$\begin{aligned}
\|r_{\Sigma,d}\|_{L^2} &\ll \left\| [u_1|u_1]_{d,0,0} \mathbf{S}^{(0)} \right\|_{L^2} \simeq \|\Sigma_d\|_{L^2}, \\
\|r_{\mathbb{V},d}\|_{L^2} &\ll \left\| [V_d u_1|u_1]_{d,-1,-1} \mathbf{S}^{(1)} \right\|_{L^2} \ll \left\| w_{AA} \mathbf{S}^{(0)} \right\|_{L^2} \simeq \|\mathbb{V}_d\|_{L^2}, \\
\|r_{\mathbb{W},d}\|_{L^2} &\ll \|\mathbf{W}_d^+\|_{L^2} \ll \left\| W_{\text{int},d}^+ \mathbb{I}_2 \right\|_{L^2} \simeq \|\mathbb{W}_d^+\|_{L^2},
\end{aligned}$$

where  $\|\mathbf{S}^{(0)}\|_{L^2} = \|\mathbf{S}^{(1)}\|_{L^2} \simeq 0.8$ . We also see that the main corrections with respect to the Bistritzer-MacDonald model come from the term  $\mathbf{W}_d^+$  defined in (73) and from the term involving  $\nabla \Sigma_d$ .

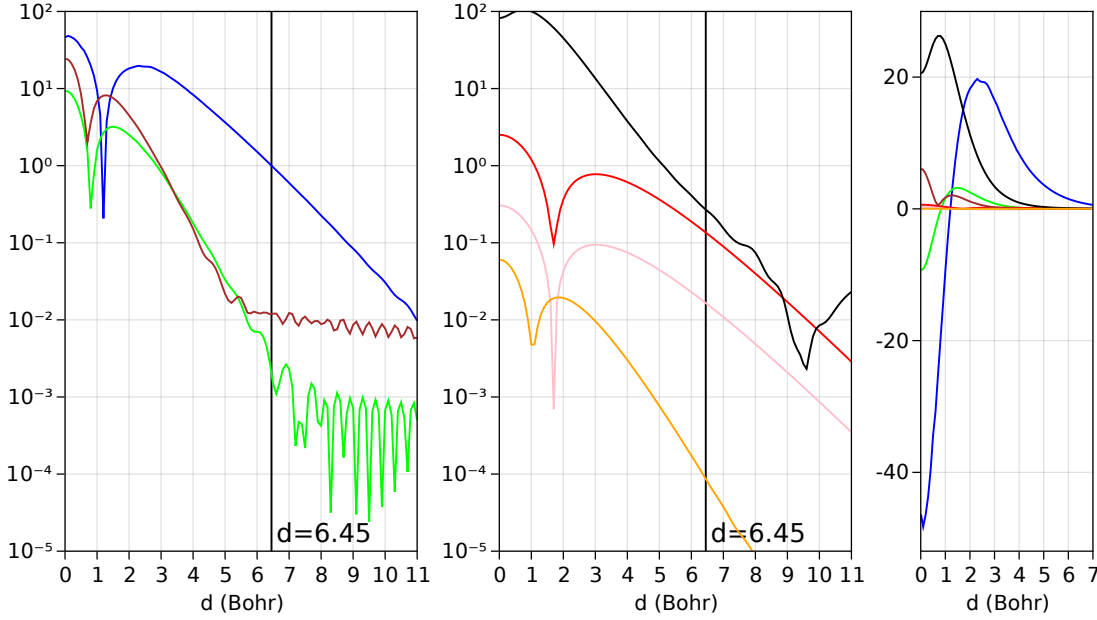


Figure 10: Variations of the reduced model parameters with respect to the interlayer distance  $d$ . Left: semi-log plots of the functions  $d \mapsto w_{AA}^d/w_{AA}^{d=6.45}$  (blue),  $d \mapsto [V_d u_1 | u_1]_{d,-1,-1}/w_{AA}^{d=6.45}$  (green),  $d \mapsto \|r_{V,d}\|_{L^2}/w_{AA}^{d=6.45}$  (brown). The oscillations of the brown and green lines for  $d > 5$  are due to numerical noise. Center: semi-log plots in log scale of  $d \mapsto \|\mathbf{W}_d^+\|_{L^2}/w_{AA}^{d=6.45}$  (black),  $d \mapsto \|\nabla \Sigma_d\|_{L^2}/v_F$  (red),  $d \mapsto \|\Sigma_d\|_{L^2}$  (pink), and  $d \mapsto \|r_{\Sigma,d}\|_{L^2}$  (orange). Right: plots of the seven functions.

## Acknowledgments

This project has received funding from the European Research Council (ERC) under the European Union's Horizon 2020 research and innovation programme (grant agreement EMC2 No 810367) and from the Simons foundation (Targeted Grant Moiré Materials Magic). The authors thank Simon Becker, Antoine Levitt, Mitchell Luskin, Allan MacDonald, Etienne Polack and Alexander Watson for useful discussions and comments. Part of this work was done during the IPAM program *Advancing quantum mechanics with mathematics and statistics*.

## Appendices

### A Formal derivation of the effective model

Our goal is to identify the leading orders terms in (28) in the limit of small twist angle. For that, we make use of the following elementary lemmas.

**Lemma 1.** *Let  $\beta \in \mathcal{S}(\mathbb{R}^2, \mathbb{C})$  and  $u \in L^1_{\text{per}}(\Omega \times \mathbb{R}; \mathbb{C})$ . Then, as  $\varepsilon \rightarrow 0$ , we have*

$$\int_{\mathbb{R}^3} \beta(\varepsilon \mathbf{x}) u(\mathbf{x}, z) d\mathbf{x} dz = \varepsilon^{-2} \left( \frac{1}{|\Omega|} \int_{\Omega \times \mathbb{R}} u \right) \int_{\mathbb{R}^2} \beta(\mathbf{X}) d\mathbf{X} + O(\varepsilon^\infty).$$

*Proof.* Expanding  $u$  as  $u(\mathbf{x}, z) = \sum_{\mathbf{G} \in \mathbb{L}^*} u_{\mathbf{G}}(z) e^{i\mathbf{G} \cdot \mathbf{x}}$  and making the change of variable

$\mathbf{X} = \varepsilon \mathbf{x}$ , we obtain

$$\begin{aligned} \int_{\mathbb{R}^3} \beta(\varepsilon \mathbf{x}) u(\mathbf{r}) d\mathbf{r} &= \varepsilon^{-2} \sum_{\mathbf{G} \in \mathbb{L}^*} \left( \int_{\mathbb{R}} u_{\mathbf{G}}(z) dz \right) \int_{\mathbb{R}} \beta(\mathbf{X}) e^{i\varepsilon^{-1} \mathbf{G} \cdot \mathbf{X}} d\mathbf{X} \\ &= \varepsilon^{-2} \sum_{\mathbf{G} \in \mathbb{L}^*} \left( \int_{\mathbb{R}} u_{\mathbf{G}}(z) dz \right) \widehat{\beta}(\varepsilon^{-1} \mathbf{G}). \end{aligned}$$

As  $\beta \in \mathcal{S}(\mathbb{R}^2; \mathbb{C})$ ,  $\widehat{\beta}$  decays faster than any polynomial. Isolating the term  $\mathbf{G} = \mathbf{0}$  gives the result.  $\square$

**Lemma 2.** *Let  $\beta \in \mathcal{S}(\mathbb{R}^2, \mathbb{C})$ ,  $\Phi, \Phi' \in L_{\mathbf{K}}^2(\Omega \times \mathbb{R}; \mathbb{C})$ , and  $\eta, \eta' \in \{\pm 1\}$ . Then, as  $\varepsilon \rightarrow 0$ , we have*

$$\int_{\mathbb{R}^3} \beta(\varepsilon_{\theta} \mathbf{x}) \left( \overline{U_{d,\theta}^{\eta} \Phi} \cdot U_{d,\theta}^{\eta'} \Phi' \right) (\mathbf{x}, z) d\mathbf{x} dz = \frac{\varepsilon_{\theta}^{-2}}{|\Omega|} \int_{\mathbb{R}^2} \beta(\mathbf{X}) \langle \Phi, \Phi' \rangle_d^{\eta\eta'}(\mathbf{X}) d\mathbf{X} + O(\varepsilon_{\theta}^{\infty}),$$

with

$$\langle \Phi, \Phi' \rangle_d^{\eta\eta'}(\mathbf{X}) := \int_{\Omega \times \mathbb{R}} \overline{\Phi(\mathbf{x} - \eta \frac{1}{2} J \mathbf{X}, z - \eta \frac{d}{2})} \Phi'(\mathbf{x} - \eta' \frac{1}{2} J \mathbf{X}, z - \eta' \frac{d}{2}) d\mathbf{x} dz.$$

In the case when  $\eta = \eta'$ , we simply have  $\langle \Phi, \Phi' \rangle_d^{\eta\eta'}(\mathbf{X}) = \langle \Phi, \Phi' \rangle_{L^2(\Omega \times \mathbb{R})}$ , so that this function is independent of  $\mathbf{X}$ . When  $\eta \neq \eta'$ , the function  $\langle \Phi, \Phi' \rangle_d^{\eta\eta'}(\mathbf{X})$  does depend on  $\mathbf{X}$  in general and is  $J\mathbb{L}$ -periodic.

Comparing  $\langle \cdot, \cdot \rangle_d$  and  $((\cdot, \cdot))_d$ , we see that if  $\Phi \in L_{\mathbf{K}}^2 = e^{i\mathbf{K} \cdot \mathbf{x}} u$  with  $u \in L_{\text{per}}^2$ , we have

$$\langle \Phi, \Phi' \rangle_d^{+-} = e^{-iJ\mathbf{K} \cdot \mathbf{X}} ((u, u'))_d^{+-}, \quad \text{and} \quad \langle \Phi, \Phi' \rangle_d^{++} = ((u, u'))_d^{++} = \langle \Phi, \Phi' \rangle = \langle u, u' \rangle.$$

In what follows, we express our quantities with  $\langle \Phi, \Phi' \rangle_d$ , but in (33)-(35), we translated our results with  $((u, u'))_d$ .

*Proof of Lemma 2.* In the case when  $\eta = \eta'$ , we have

$$\begin{aligned} \int_{\mathbb{R}^3} \beta(\varepsilon_{\theta} \mathbf{x}) \left( \overline{U_{d,\theta}^{\eta} \Phi} \cdot U_{d,\theta}^{\eta'} \Phi' \right) (\mathbf{x}, z) d\mathbf{x} dz &= \int_{\mathbb{R}^3} \beta(\varepsilon_{\theta} \mathbf{x}) (\overline{\Phi} \Phi') \left( R_{-\eta \frac{\theta}{2}} \mathbf{x}, z - \eta \frac{d}{2} \right) d\mathbf{x} dz \\ &= \varepsilon_{\theta}^{-2} \int_{\mathbb{R}^3} \beta(\mathbf{X}) (\overline{\Phi} \Phi') \left( \varepsilon_{\theta}^{-1} R_{-\eta \frac{\theta}{2}} \mathbf{X}, z \right) d\mathbf{X} dz. \end{aligned}$$

As the function  $\overline{\Phi} \Phi'$  is  $\mathbb{L}$ -periodic, the result can be obtained by applying the same arguments as in the proof of Lemma 1.

Let us now focus on the case when  $\eta \neq \eta'$ , and prove the result for  $\eta' = +1$  and  $\eta = -1$ , the other case being similar. Let  $u(\mathbf{r}) := e^{-i\mathbf{K} \cdot \mathbf{x}} \Phi(\mathbf{r})$  and  $u'(\mathbf{r}) := e^{-i\mathbf{K} \cdot \mathbf{x}} \Phi'(\mathbf{r})$  be the periodic components of the Bloch waves  $\Phi$  and  $\Phi'$  respectively. We have

$$\left( \overline{U_{d,\theta} \Phi} \cdot U_{d,\theta}^{-1} \Phi' \right) (\mathbf{x}, z) = e^{i\mathbf{K} \varepsilon_{\theta} \cdot J \mathbf{x}} \overline{u(c_{\theta} \mathbf{x} - \frac{1}{2} \varepsilon_{\theta} J \mathbf{x}, z - \frac{d}{2})} u'(c_{\theta} \mathbf{x} + \frac{1}{2} \varepsilon_{\theta} J \mathbf{x}, z + \frac{d}{2}).$$

Introducing the Fourier expansions of the functions  $u$  and  $u'$ , this is also

$$\frac{1}{|\Omega|} \sum_{\mathbf{G}, \mathbf{G}' \in \mathbb{L}^*} \left[ \overline{u_{\mathbf{G}}}(z - \frac{d}{2}) u'_{\mathbf{G}'}(z + \frac{d}{2}) e^{i(\mathbf{G}' - \mathbf{G}) \cdot c_{\theta} \mathbf{x}} \right] e^{i \frac{1}{2} (\mathbf{G} + \mathbf{G}' + 2\mathbf{K}) \varepsilon_{\theta} \cdot J \mathbf{x}}.$$

Note that the last phase factor varies at the moiré scale. The term in brackets is a  $c_\theta^{-1}\mathbb{L}$ -periodic function with zero mean unless  $\mathbf{G} = \mathbf{G}'$ . Reasoning as above, we obtain

$$\begin{aligned} & \int_{\mathbb{R}^3} \beta(\varepsilon_\theta \mathbf{x}) \left( \overline{U_{d,\theta}^\eta \Phi} \cdot U_{d,\theta}^{\eta'} \Phi' \right) (\mathbf{x}, z) \, d\mathbf{x} \, dz = \\ &= \frac{\varepsilon_\theta^{-2}}{|\Omega|} \int_{\mathbb{R}^2} \beta(\mathbf{X}) \left[ e^{i\mathbf{K} \cdot J\mathbf{X}} \sum_{\mathbf{G} \in \mathbb{L}^*} \left( \int_{\mathbb{R}} \overline{u_{\mathbf{G}}}(z - \frac{d}{2}) u'_{\mathbf{G}}(z + \frac{d}{2}) \, dz \right) e^{i\mathbf{G} \cdot J\mathbf{X}} \right] d\mathbf{X} + O(\varepsilon_\theta^\infty). \end{aligned}$$

Finally, by Parseval theorem, the term in brackets is equal to  $\langle\langle \Phi, \Phi' \rangle\rangle_d^{\eta\eta'}(\mathbf{X})$ , which proves the result.  $\square$

## A.1 Effective overlap operator

Let us first focus on the left-hand side of (28). Setting  $\Phi_{\eta j} := U_{d,\theta}^\eta \Phi_j$ , we have

$$\left\langle (\tilde{\alpha} : \Phi)_{d,\theta}, (\alpha(\varepsilon_\theta t) : \Phi)_{d,\theta} \right\rangle = \sum_{\substack{\eta, \eta' \in \{\pm 1\} \\ j, j' \in \{1, 2\}}} \int_{\mathbb{R}^3} \left( \overline{\tilde{\alpha}_{\eta j}} \alpha_{\eta' j'}(t) \right) (\varepsilon_\theta \mathbf{x}) \times (\overline{\Phi_{\eta' j'}} \Phi_{\eta j}) (\mathbf{x}, z) \, d\mathbf{x} \, dz.$$

Using directly Lemma 2 (with  $\beta = \overline{\tilde{\alpha}_{\eta j}} \alpha_{\eta' j'}$ ), we obtain that this term equals

$$\varepsilon_\theta^{-2} \sum_{\substack{\eta, \eta' \in \{\pm 1\} \\ j, j' \in \{1, 2\}}} \int_{\mathbb{R}^2} \left( \overline{\tilde{\alpha}_{\eta j}} \alpha_{\eta' j'}(\varepsilon_\theta t) \right) (\mathbf{X}) \langle\langle \Phi_j, \Phi_{j'} \rangle\rangle_d^{\eta\eta'}(\mathbf{X}) \, d\mathbf{X} + O(\varepsilon^\infty).$$

Ranking the components of  $\alpha$  as  $\alpha = (\alpha_{+,1}, \alpha_{+,2}, \alpha_{-,1}, \alpha_{-,2})^T$  (the first two entries correspond to the top layer, the last two to the bottom one), we obtain

$$\frac{d}{dt} \left\langle (\tilde{\alpha} : \Phi)_{d,\theta}, (\alpha(\varepsilon_\theta t) : \Phi)_{d,\theta} \right\rangle = \frac{\varepsilon_\theta^{-1}}{|\Omega|} \langle \tilde{\alpha}, \mathcal{S}_d \partial_\tau \alpha(\varepsilon_\theta t) \rangle_{L^2(\mathbb{R}^2; \mathbb{C}^4)} + O(\varepsilon_\theta^\infty),$$

with

$$\mathcal{S}_d = \begin{pmatrix} \mathbb{I}_2 & \Sigma_d(\mathbf{X}) \\ \Sigma_d^*(\mathbf{X}) & \mathbb{I}_2 \end{pmatrix}, \quad [\Sigma_d]_{jj'}(\mathbf{X}) := \langle\langle \Phi_j, \Phi_{j'} \rangle\rangle_d^{+-}(\mathbf{X}).$$

## A.2 Effective Hamiltonian operator

We now focus on the terms on the right-hand side. First, we record that

$$\begin{aligned} & (-\tfrac{1}{2}\Delta_{\mathbf{r}}) [\beta(\varepsilon_\theta \mathbf{x}) \varphi(\mathbf{r})] = \\ &= \varepsilon_\theta^2 (-\tfrac{1}{2}\Delta \beta)(\varepsilon_\theta \mathbf{x}) \varphi(\mathbf{r}) + \varepsilon_\theta (-i\nabla \beta)(\varepsilon_\theta \mathbf{x}) \cdot (-i\nabla_{\mathbf{x}} \varphi)(\mathbf{r}) + \beta(\varepsilon_\theta \mathbf{x}) (-\tfrac{1}{2}\Delta \varphi)(\mathbf{r}). \end{aligned} \quad (74)$$

This gives

$$\left\langle (\tilde{\alpha} : \Phi)_{d,\theta}, \left( H_{d,\theta}^{(2)} - \mu_F \right) (\alpha : \Phi)_{d,\theta} \right\rangle = g_1 + g_2 + g_3,$$

with

$$\begin{aligned} g_1 &:= \varepsilon_\theta^2 \sum_{\substack{\eta, \eta' \in \{\pm 1\} \\ j, j' \in \{1, 2\}}} \int_{\mathbb{R}^3} \left[ \overline{\tilde{\alpha}_{\eta, j}} (-\tfrac{1}{2}\Delta \alpha_{\eta', j'}) \right] (\varepsilon_\theta \mathbf{x}) (\overline{\Phi_{\eta, j}} \Phi_{\eta', j'}) (\mathbf{r}) \, d\mathbf{r}, \\ g_2 &:= \varepsilon_\theta \sum_{\substack{\eta, \eta' \in \{\pm 1\} \\ j, j' \in \{1, 2\}}} \int_{\mathbb{R}^3} \left[ \overline{\tilde{\alpha}_{\eta, j}} (-i\nabla \alpha_{\eta', j'}) \right] (\varepsilon_\theta \mathbf{x}) \cdot [\overline{\Phi_{\eta, j}} (-i\nabla_{\mathbf{x}} \Phi_{\eta', j'})] (\mathbf{r}) \, d\mathbf{r}, \end{aligned}$$

$$g_3 := \sum_{\substack{\eta, \eta' \in \{\pm 1\} \\ j, j' \in \{1, 2\}}} \int_{\mathbb{R}^3} \left[ \overline{\tilde{\alpha}_{\eta, j} \alpha_{\eta', j'}(\varepsilon_\theta \mathbf{x})} \right] \cdot \left[ \bar{\Phi}_{\eta, j} \times (H_{d, \theta}^{(2)} - \mu_F) \Phi_{\eta', j'} \right] (\mathbf{r}) d\mathbf{r}.$$

For the first term  $g_1$ , we apply directly Lemma 2, which gives

$$g_1 = \frac{1}{|\Omega|} \sum_{\substack{\eta, \eta' \in \{\pm 1\} \\ j, j' \in \{1, 2\}}} \int_{\mathbb{R}^2} \left( \overline{\tilde{\alpha}_{\eta j}} (-\tfrac{1}{2} \Delta \alpha_{\eta' j'}) \right) (\mathbf{X}) \langle \Phi_j, \Phi_{j'} \rangle_d^{\eta \eta'} (\mathbf{X}) d\mathbf{X} + O(\varepsilon_\theta^\infty).$$

This term can be written as  $g_1 = |\Omega|^{-1} \langle \tilde{\alpha}, G_1 \alpha \rangle + O(\varepsilon_\theta^\infty)$  with

$$G_1 := \mathcal{S}_d(\mathbf{X}) (-\tfrac{1}{2} \Delta).$$

For the second term  $g_2$ , we first notice that

$$(-i \nabla_{\mathbf{x}} \Phi_{\eta', j'}) (\mathbf{r}) = (-i \nabla_{\mathbf{x}}) \left[ \Phi_{j'} (R_{\theta/2}^{-\eta'} \mathbf{x}, z - \eta' \tfrac{d}{2}) \right] = R_{\theta/2}^{\eta'} \left[ U_{d, \theta}^{\eta'} (-i \nabla_{\mathbf{x}} \Phi_{j'}) \right] (\mathbf{r}).$$

This gives, using arguments similar to the ones of Lemma 2,

$$g_2 = \frac{1}{|\Omega|} \sum_{\substack{\eta, \eta' \in \{\pm 1\} \\ j, j' \in \{1, 2\}}} \varepsilon_\theta^{-1} \int_{\mathbb{R}^2} \left( \overline{\tilde{\alpha}_{\eta j}} (-i \nabla \alpha_{\eta' j'}) \right) (\mathbf{X}) \cdot R_{\theta/2}^{\eta'} \langle \Phi_j, (-i \nabla_{\mathbf{x}} \Phi_{j'}) \rangle_d^{\eta \eta'} (\mathbf{X}) d\mathbf{X} + O(\varepsilon_\theta^\infty).$$

To deal with the diagonal terms  $\eta = \eta'$ , we use (9). Regarding the off-diagonal terms (here for  $\eta = +1$  and  $\eta' = -1$ ), we have, using that  $J^T = -J$ ,

$$\begin{aligned} \nabla \langle \Phi, \Phi' \rangle_d^{+-} (\mathbf{X}) &= \tfrac{1}{2} J \int_{\Omega \times \mathbb{R}} \overline{(\nabla_{\mathbf{x}} \Phi) \left( \mathbf{x} - \tfrac{1}{2} J \mathbf{X}, z - \tfrac{d}{2} \right)} \Phi' \left( \mathbf{x} + \tfrac{1}{2} J \mathbf{X}, z + \tfrac{d}{2} \right) d\mathbf{x} dz \\ &\quad - \tfrac{1}{2} J \int_{\Omega \times \mathbb{R}} \overline{\Phi \left( \mathbf{x} - \tfrac{1}{2} J \mathbf{X}, z - \tfrac{d}{2} \right)} (\nabla_{\mathbf{x}} \Phi') \left( \mathbf{x} + \tfrac{1}{2} J \mathbf{X}, z + \tfrac{d}{2} \right) d\mathbf{x} dz. \end{aligned}$$

Integrating by part the first term in the RHS, and multiplying by  $(-i)$  gives

$$(-i \nabla) \langle \Phi, \Phi' \rangle_d^{+-} = -J \langle \Phi, (-i \nabla_{\mathbf{x}}) \Phi' \rangle_d^{+-}, \quad \text{hence} \quad \langle \Phi, (-i \nabla_{\mathbf{x}}) \Phi' \rangle_d^{+-} = J (-i \nabla) \langle \Phi, \Phi' \rangle_d^{+-}.$$

Similarly, in the case  $\eta = -1$  and  $\eta' = 1$ , we have

$$\langle \Phi, (-i \nabla_{\mathbf{x}}) \Phi' \rangle_d^{-+} = -J (-i \nabla) \langle \Phi, \Phi' \rangle_d^{-+}.$$

Recalling the definition of  $\Sigma_d$  in (31), we obtain that  $g_2 = |\Omega|^{-1} \langle \tilde{\alpha}, G_2 \alpha \rangle + O(\varepsilon_\theta^\infty)$  with (we use that  $R_{\theta/2} = c_\theta \mathbb{I}_2 + \tfrac{1}{2} \varepsilon_\theta J$  in the second line)

$$\begin{aligned} G_2 &= \frac{1}{\varepsilon_\theta} \begin{pmatrix} v_F \boldsymbol{\sigma} \cdot [R_{-\theta/2} (-i \nabla)] & J (-i \nabla \Sigma_d) (\mathbf{X}) \cdot [R_{\theta/2} (-i \nabla)] \\ J (-i \nabla \Sigma_d^*) (\mathbf{X}) \cdot [R_{-\theta/2} (-i \nabla)] & v_F \boldsymbol{\sigma} \cdot [R_{\theta/2} (-i \nabla)] \end{pmatrix} \\ &= \frac{c_\theta}{\varepsilon_\theta} \begin{pmatrix} v_F \boldsymbol{\sigma} \cdot (-i \nabla) & J (-i \nabla \Sigma_d) (\mathbf{X}) \cdot (-i \nabla) \\ J (-i \nabla \Sigma_d^*) (\mathbf{X}) \cdot (-i \nabla) & v_F \boldsymbol{\sigma} \cdot (-i \nabla) \end{pmatrix} \\ &\quad + \frac{1}{2} \begin{pmatrix} -v_F \boldsymbol{\sigma} \cdot [J (-i \nabla)] & (-i \nabla \Sigma_d) (\mathbf{X}) \cdot (-i \nabla) \\ (-i \nabla \Sigma_d^*) (\mathbf{X}) \cdot (-i \nabla) & v_F \boldsymbol{\sigma} \cdot [J (-i \nabla)] \end{pmatrix}. \end{aligned}$$

Finally, for the term  $g_3$ , we use that  $\Phi_j$  is an eigenvector of the single-layer graphene Hamiltonian  $H^{(1)}$  associated with the eigenvalue  $\mu_F$  and get

$$\left[ (H_{d, \theta}^{(2)} - \mu_F) \Phi_{\eta, j} \right] (\mathbf{r}) = \left( U_{d, \theta}^{-\eta} V \right) (\mathbf{r}) \Phi_{\eta, j} (\mathbf{r}) + V_{\text{int}, d}(z) \Phi_{\eta, j} (\mathbf{r}),$$

and

$$g_3 = \sum_{\substack{\eta', \eta \in \{\pm 1\} \\ j', j \in \{1, 2\}}} \int_{\mathbb{R}^3} \left[ \overline{(\tilde{\alpha}_{\eta', j'} \alpha_{\eta, j})} (\varepsilon_\theta \mathbf{x}) \right] \cdot \left[ \left( U_{d, \theta}^{-\eta} V \right) \bar{\Phi}_{\eta', j'} \Phi_{\eta, j} + V_{\text{int}, d} \bar{\Phi}_{\eta', j'} \Phi_{\eta, j} \right] (\mathbf{r}) d\mathbf{r}.$$

Using reasoning similar to the proof of Lemma 2, we obtain that  $g_3 = \langle \tilde{\alpha}, G_3 \alpha \rangle + O(\varepsilon_\theta^\infty)$ , with

$$G_3 = \varepsilon_\theta^{-2} \begin{pmatrix} \mathbb{W}_d^+(\mathbf{X}) & \mathbb{V}_d(\mathbf{X}) \\ \mathbb{V}_d(\mathbf{X})^* & \mathbb{W}_d^-(\mathbf{X}) \end{pmatrix},$$

where

$$\begin{aligned} [\mathbb{V}_d(\mathbf{X})]_{jj'} &= \langle V \Phi_j, \Phi_{j'} \rangle_d^{+-}(\mathbf{X}) + \int_{\Omega \times \mathbb{R}} \overline{\Phi_j \left( \mathbf{x} - \frac{1}{2} J \mathbf{X}, z - \frac{d}{2} \right)} \Phi_{j'} \left( \mathbf{x} + \frac{1}{2} J \mathbf{X}, z + \frac{d}{2} \right) V_{\text{int}, d}(z) d\mathbf{r}, \\ [\mathbb{W}_d^\pm(\mathbf{X})]_{jj'} &= ((\Phi_j \bar{\Phi}_{j'}, V))_d^{\pm\mp}(\mathbf{X}) + \int_{\Omega \times \mathbb{R}} (\bar{\Phi}_j \Phi_{j'}) (\mathbf{x}, z \mp \frac{d}{2}) V_{\text{int}, d}(z) d\mathbf{r}, \end{aligned}$$

where we recall that the notation  $((f, g))_d$  was defined in (36), and is used when  $f$  and  $g$  are periodic.

The second term of  $\mathbb{W}_d^\pm$  is a constant matrix (independent of  $\mathbf{X}$ ). Using computations similar to (8) (that is, applying rotations), we can see that this term is diagonal, and applying the  $\mathcal{CP}$  and  $\mathcal{S}$  symmetries, that this matrix is proportional to  $\mathbb{I}_2$ . Finally, since  $V_{\text{int}, d}(-z) = V_{\text{int}, d}(z)$ , this matrix is the same for the  $\mathbb{W}_d^+$  and the  $\mathbb{W}_d^-$  terms.

To conclude and obtain the above expression of  $T_d^{(1)}$  in (32), we have used the equality

$$\Sigma_d(-\frac{1}{2}\Delta) + \frac{1}{2}(-i\nabla \Sigma_d) \cdot (-i\nabla) = -\frac{1}{2} \text{div}(\Sigma_d(\mathbf{X}) \nabla \bullet).$$

## B TBG Hamiltonians with nonlocal pseudopotentials

In the presence of norm-conserving pseudopotentials, the TBG approximate Kohn-Sham Hamiltonian contains an additional term originating from the nonlocal contribution to the pseudopotential:

$$H_{\theta, d}^{(2)} := -\frac{1}{2}\Delta + V_{d, \theta}^{(2)} + U_{d, \theta} V_{\text{nl}} U_{d, \theta}^{-1} + U_{d, \theta}^{-1} V_{\text{nl}} U_{d, \theta}.$$

Here,  $V_{d, \theta}^{(2)}$  is a local potential of the form (17) where  $V$  is the *local component* of the Kohn-Sham potential of single-layer graphene,

$$V_{d, \theta}^{(2)}(\mathbf{x}, z) := (U_{d, \theta} V)(\mathbf{x}, z) + (U_{d, \theta}^* V)(\mathbf{x}, z) + V_{\text{int}, d}(z),$$

and  $V_{\text{nl}}$  the  $\mathbb{L}$ -periodic nonlocal component of the pseudopotential of single-layer graphene. For the Goedecker-Teter-Hutter pseudopotential implemented in the DFTK software used in our numerical simulations,  $V_{\text{nl}}$  is of the form

$$V_{\text{nl}} = v_0 \sum_{\mathbf{R} \in \mathfrak{C}} |\tau_{\mathbf{R}} \varphi\rangle \langle \tau_{\mathbf{R}} \varphi|, \quad \tau_{\mathbf{R}} \varphi := \varphi(\cdot - \mathbf{R}),$$

where  $v_0 > 0$ , and where  $\mathfrak{C} := (\mathbb{L} + \mathbf{b}_1) \cup (\mathbb{L} + \mathbf{b}_2)$  denotes the locations of the Carbon atoms in graphene. Here,  $\mathbf{b}_1 := \frac{2}{3}\mathbf{a}_1 + \frac{1}{3}\mathbf{a}_2$ ,  $\mathbf{b}_2 := \frac{1}{3}\mathbf{a}_1 + \frac{2}{3}\mathbf{a}_2$  are the positions of the atom in the Wigner-Seitz cell, and  $\varphi$  is a radial normalized Gaussian function with variance similar to the characteristic radius of the carbon 1s orbital.

The functions  $\Phi_j$  satisfy

$$\left(-\frac{1}{2}\Delta + V + V_{\text{nl}} - \mu_{\text{F}}\right) \Phi_j = 0.$$

Actually, since  $\varphi$  is even while  $\Phi_j$  is odd with respect to the horizontal symmetry plane, we have  $\langle \varphi, \Phi_j \rangle = 0$ , hence  $V_{\text{nl}}\Phi_j = 0$ , and  $\Phi_j$  also satisfies

$$\left(-\frac{1}{2}\Delta + V - \mu_{\text{F}}\right) \Phi_j = 0.$$

We need to compute  $H_{\theta,d}^{(2)}(\alpha : \Phi)_{d,\theta}$ . For the Laplacian part, we can still use (74), and the local part of the potential can still act directly on the Bloch modes. We only need to focus on the non-local part of the potential. We have

$$\begin{aligned} & \left\langle (\tilde{\alpha} : \Phi)_{d,\theta} \left| \left( U_{d,\theta} V_{\text{nl}} U_{d,\theta}^{-1} + U_{d,\theta}^{-1} V_{\text{nl}} U_{d,\theta} \right) \right| (\alpha : \Phi)_{d,\theta} \right\rangle \\ &= \sum_{\eta,j} \sum_{\eta',j'} \sum_{\eta''} \langle \tilde{\alpha}_{\eta,j}(\varepsilon_{\theta} \cdot) U_{d,\theta}^{\eta} \Phi_j | U_{d,\theta}^{\eta''} V_{\text{nl}} U_{d,\theta}^{-\eta''} | \alpha_{\eta',j'}(\varepsilon_{\theta} \cdot) U_{d,\theta}^{\eta'} \Phi_{j'} \rangle \\ &= v_0 \sum_{\eta,j} \sum_{\eta',j'} \sum_{\eta''} \sum_{\mathbf{R}} \langle U_{d,\theta}^{-\eta''} (\tilde{\alpha}_{\eta,j}(\varepsilon_{\theta} \cdot) U_{d,\theta}^{\eta} \Phi_j) | \tau_{\mathbf{R}} \varphi \rangle \langle \tau_{\mathbf{R}} \varphi | U_{d,\theta}^{-\eta''} (\alpha_{\eta',j'}(\varepsilon_{\theta} \cdot) U_{d,\theta}^{\eta'} \Phi_{j'}) \rangle. \end{aligned} \quad (75)$$

Again, since  $\varphi$  is even and  $\Phi_j$  is odd with respect to the horizontal symmetry plane, we have that for all  $\mathbf{R}, \eta, j$ ,

$$\langle \tau_{\mathbf{R}} \varphi | U_{d,\theta}^{-\eta} (\beta(\varepsilon_{\theta} \cdot) U_{d,\theta}^{\eta} \Phi_j) \rangle = 0.$$

Thus only the contribution  $\eta'' = -\eta' = -\eta$  contributes to the sum, which reduces to

$$v_0 \sum_{\eta} \sum_{j,j'} \sum_{\mathbf{R}} \langle U_{d,\theta}^{\eta} (\tilde{\alpha}_{\eta,j}(\varepsilon_{\theta} \cdot) U_{d,\theta}^{\eta} \Phi_j) | \tau_{\mathbf{R}} \varphi \rangle \langle \tau_{\mathbf{R}} \varphi | U_{d,\theta}^{\eta} (\alpha_{\eta,j'}(\varepsilon_{\theta} \cdot) U_{d,\theta}^{\eta} \Phi_{j'}) \rangle.$$

We now compute the above inner products. We have

$$\begin{aligned} & \langle \tau_{\mathbf{R}} \varphi | U_{d,\theta}^{\eta} (\beta(\varepsilon_{\theta} \cdot) U_{d,\theta}^{\eta} \Phi_j) \rangle \\ &= \int_{\mathbb{R}^3} \beta \left( \varepsilon_{\theta} R_{\frac{\eta}{2}}^* \mathbf{x} \right) \overline{\varphi(\mathbf{x} - \mathbf{R}, z)} \Phi_j \left( R_{\eta\theta}^* \mathbf{x}, z - \eta d \right) d\mathbf{x} dz \\ &= \int_{\mathbb{R}^3} \beta \left( \varepsilon_{\theta} R_{\frac{\eta}{2}}^* (\mathbf{y} + \mathbf{R}) \right) \overline{\varphi(\mathbf{y}, z)} \Phi_j \left( R_{\eta\theta}^* (\mathbf{y} + \mathbf{R}), z - \eta d \right) d\mathbf{y} dz \\ &= \int_{\mathbb{R}^3} \beta \left( \varepsilon_{\theta} R_{\frac{\eta}{2}}^* \mathbf{R} + \varepsilon_{\theta} R_{\frac{\eta}{2}} \mathbf{y} \right) \overline{\varphi(\mathbf{y}, z)} \Phi_j \left( R_{\eta\theta}^* \mathbf{R} + \mathbf{y}, z - \eta d \right) d\mathbf{y} dz, \end{aligned}$$

where we used that  $\varphi$  is radially symmetric in the last line. Since  $\varphi$  is localized near  $\mathbf{y} = \mathbf{0}$ , we perform a Taylor expansion of  $\beta$  in  $\mathbf{y}$ . This one takes the form

$$\beta \left( \varepsilon_{\theta} R_{\frac{\eta}{2}}^* \mathbf{R} + \varepsilon_{\theta} R_{\frac{\eta}{2}} \mathbf{y} \right) = \beta \left( \varepsilon_{\theta} R_{\frac{\eta}{2}}^* \mathbf{R} \right) + \varepsilon_{\theta} \nabla \beta \left( \varepsilon_{\theta} R_{\frac{\eta}{2}}^* \mathbf{R} \right) \cdot R_{\frac{\eta}{2}} \mathbf{y} + \dots$$

We obtain a series in  $\varepsilon_{\theta}$ , whose first terms are given by

$$\langle \tau_{\mathbf{R}} \varphi | U_{d,\theta}^{\eta} (\beta(\varepsilon_{\theta} \cdot) U_{d,\theta}^{\eta} \Phi_j) \rangle = \beta \left( \varepsilon_{\theta} R_{\frac{\eta}{2}}^* \mathbf{R} \right) F_{0,j}(R_{\eta\theta}^* \mathbf{R}) + \varepsilon_{\theta} R_{\frac{\eta}{2}}^* \nabla \beta \left( \varepsilon_{\theta} R_{\frac{\eta}{2}}^* \mathbf{R} \right) \cdot G_{1,j}(R_{\eta\theta}^* \mathbf{R}) + \dots$$

where

$$\begin{aligned} F_{0,j}(\mathbf{X}) &:= \int_{\mathbb{R}^3} \overline{\varphi(\mathbf{y}, z)} \Phi_j(\mathbf{X} + \mathbf{y}, z - \eta d) d\mathbf{y} dz, \\ G_{1,j}(\mathbf{X}) &:= \int_{\mathbb{R}^3} \mathbf{y} \overline{\varphi(\mathbf{y}, z)} \Phi_j(\mathbf{X} + \mathbf{y}, z - \eta d) d\mathbf{y} dz. \end{aligned}$$

We can go on with the Taylor expansion, but we stop here, as the leading order is already enough for numerical purpose (we show below that even the leading order term can be neglected). The leading order term of (75) is therefore

$$v_0 \sum_{\eta,j,j'} \sum_{\mathbf{R} \in \mathfrak{C}} (\overline{\alpha_{\eta,j}} \alpha_{\eta,j'}) \left( \varepsilon_\theta R_{\eta/2}^* \mathbf{R} \right) \left[ \overline{F_{0,j}} F_{0,j'} \right] (R_{\eta\theta}^* \mathbf{R}).$$

Assuming that the  $\alpha$ -functions are in the Schwartz class, and performing a Taylor expansion in  $\varepsilon_\theta$  of the  $F$ -functions using the equality  $R_{\eta\theta}^* = c_\theta - 2\varepsilon_\theta \eta J = 1 - 2\varepsilon_\theta \eta J + O(\varepsilon_\theta^2)$ , we obtain, for  $s \in \{1, 2\}$  and  $\mathbf{R} \in \mathbb{L}$ ,

$$\begin{aligned} F_{0,j}(R_{\eta\theta}^*(\mathbf{R} + \mathbf{b}_s)) &\approx F_{0,j}((\mathbf{R} + \mathbf{b}_s) - 2\varepsilon_\theta \eta J(\mathbf{R} + \mathbf{b}_s)) \\ &= \int_{\mathbb{R}^3} \overline{\varphi(\mathbf{y}, z)} \Phi_j(\mathbf{R} + \mathbf{b}_s - 2\varepsilon_\theta \eta J(\mathbf{R} + \mathbf{b}_s) + \mathbf{y}, z - \eta d) \, d\mathbf{y} dz \\ &= e^{i\mathbf{K} \cdot \mathbf{R}} \tilde{F}_{0,s,j,\eta}(\varepsilon_\theta(\mathbf{R} + \mathbf{b}_s)), \end{aligned}$$

with

$$\tilde{F}_{0,s,j,\eta}(\mathbf{X}) := \int_{\mathbb{R}^3} \overline{\varphi(\mathbf{y}, z)} \Phi_j(\mathbf{b}_s - 2\eta J\mathbf{X} + \mathbf{y}, z - \eta d) \, d\mathbf{y} dz.$$

Performing a similar expansion for the  $\alpha$ -functions gives, to leading order,

$$v_0 \sum_{\eta,j,j'} \sum_{s \in \{1,2\}} \sum_{\mathbf{R} \in \mathbb{L}} (\overline{\alpha_{\eta,j}} \alpha_{\eta,j'}) (\varepsilon_\theta(\mathbf{R} + \mathbf{b}_s)) \left[ \overline{\tilde{F}_{0,s,j}} \tilde{F}_{0,s,j'} \right] (\varepsilon_\theta(\mathbf{R} + \mathbf{b}_s)).$$

We recognize a Riemann sum. Therefore, at leading order, this term also equals (the superscript  $-1$  refers to the fact that only the leading order term was taken into account)

$$\frac{1}{\varepsilon_\theta^2} \sum_{\eta,j,j'} \int_{\mathbb{R}^2} (\overline{\alpha_{\eta,j}} \alpha_{\eta,j'}) (\mathbf{X}) [\mathbb{W}_d^{\text{nl},-1}]_{jj'}(\mathbf{X}) d\mathbf{X}, \quad \text{with} \quad [\mathbb{W}_d^{\text{nl},-1}]_{jj'} := v_0 \sum_{s \in \{1,2\}} \overline{\tilde{F}_{0,s,j}} \tilde{F}_{0,s,j'}.$$

This term modifies the effective Hamiltonian as follows:

$$\mathcal{H}_{d,\theta}^{\text{nl},-1} = \varepsilon_\theta^{-1} \left( \mathcal{V}_d + \mathcal{V}_d^{\text{nl},-1} \right) + c_\theta T_d + \varepsilon_\theta T_d^{(1)}, \quad (76)$$

where

$$\mathcal{V}_d^{\text{nl},-1} := \begin{pmatrix} \mathbb{W}_d^{\text{nl},-1} & 0 \\ 0 & \mathbb{W}_d^{\text{nl},-1} \end{pmatrix}. \quad (77)$$

The remainder in the three-term expansion (30) valid for local (multiplicative) potentials is of order  $\varepsilon_\theta^\infty$ . In contrast, the non-local component of the pseudopotential gives rise to an infinite series of terms of orders  $\varepsilon_\theta^k$  for all  $k \geq -1$ . Fortunately, all these terms, including the leading order one (see Fig. 11) are very small ( $\sim 4 \times 10^{-4}$  meV) and can be neglected.



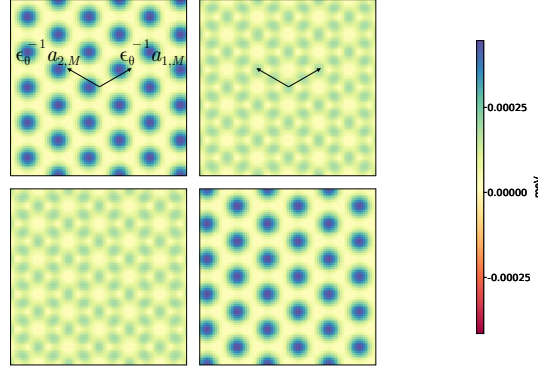


Figure 11: Moduli of the 4 entries of the matrix-valued function  $\mathbb{W}_d^{\text{nl},-1}(\mathbf{X})$ .

## References

- [1] E. Y. Andrei et al. “The marvels of moiré materials”. In: *Nature Reviews Materials* 6.3 (2021), pp. 201–206.
- [2] S. Becker et al. “Spectral characterization of magic angles in twisted bilayer graphene”. In: *Phys. Rev. B* 103 (16 2021), p. 165113.
- [3] B. A. Bernevig et al. “Twisted bilayer graphene. I. Matrix elements, approximations, perturbation theory, and a  $k \cdot p$  two-band model”. In: *Phys. Rev. B* 103 (20 2021), p. 205411.
- [4] J. Bezanson et al. “Julia: A Fresh Approach to Numerical Computing”. In: *SIAM Rev.* 59.1 (2017), pp. 65–98.
- [5] R. Bistritzer and A. H. MacDonald. “Moiré butterflies in twisted bilayer graphene”. In: *Phys. Rev. B* 84 (3 2011), p. 035440.
- [6] R. Bistritzer and A. H. MacDonald. “Moiré bands in twisted double-layer graphene”. In: *Proceedings of the National Academy of Sciences* 108.30 (2011), pp. 12233–12237.
- [7] É. Cancès, S. Lahbabi, and M. Lewin. “Mean-field models for disordered crystals”. In: *Journal de Mathématiques Pures et Appliquées* 100.2 (2013), pp. 241–274.
- [8] Y. Cao et al. “Unconventional superconductivity in magic-angle graphene superlattices”. In: *Nature* 556.7699 (2018), pp. 43–50.
- [9] S. Carr, S. Fang, and E. Kaxiras. “Electronic-structure methods for twisted moiré layers”. In: *Nature Reviews Materials* 5.10 (2020), pp. 748–763.
- [10] S. Carr et al. “Exact continuum model for low-energy electronic states of twisted bilayer graphene”. In: *Phys. Rev. Research* 1 (1 2019), p. 013001.
- [11] S. Carr et al. “Pressure dependence of the magic twist angle in graphene superlattices”. In: *Phys. Rev. B* 98 (8 2018), p. 085144.
- [12] S. Carr et al. “Relaxation and domain formation in incommensurate two-dimensional heterostructures”. In: *Phys. Rev. B* 98 (22 2018), p. 224102.
- [13] S. Carr et al. “Twistronics: Manipulating the electronic properties of two-dimensional layered structures through their twist angle”. In: *Phys. Rev. B* 95 (7 2017), p. 075420.
- [14] P. Cazeaux, M. Luskin, and D. Massatt. “Energy Minimization of Two Dimensional Incommensurate Heterostructures”. In: *Archive for Rational Mechanics and Analysis* 235.2 (2020), pp. 1289–1325.

- [15] S. Fang et al. “Angle-Dependent Ab initio Low-Energy Hamiltonians for a Relaxed Twisted Bilayer Graphene Heterostructure”.
- [16] C. L. Fefferman and M. I. Weinstein. “Wave Packets in Honeycomb Structures and Two-Dimensional Dirac Equations”. In: *Communications in Mathematical Physics* 326.1 (2013), pp. 251–286.
- [17] M. F. Herbst, A. Levitt, and E. Cancès. “DFTK: A Julian approach for simulating electrons in solids”. In: *Proceedings of the JuliaCon Conferences*. Vol. 3. 26. 2021, p. 69.
- [18] J. Jung and A. H. MacDonald. “Accurate tight-binding models for the  $\pi$  bands of bilayer graphene”. In: *Phys. Rev. B* 89 (3 2014), p. 035405.
- [19] M. Koshino and N. N. T. Nam. “Effective continuum model for relaxed twisted bilayer graphene and moiré electron-phonon interaction”. In: *Phys. Rev. B* 101 (19 2020), p. 195425.
- [20] G. Trambly de Laissardière, D. Mayou, and L. Magaud. “Numerical studies of confined states in rotated bilayers of graphene”. In: *Phys. Rev. B* 86 (12 2012), p. 125413.
- [21] H. A. Le and V. N. Do. “Electronic structure and optical properties of twisted bilayer graphene calculated via time evolution of states in real space”. In: *Phys. Rev. B* 97 (12 2018), p. 125136.
- [22] E. J. Mele. “Commensuration and interlayer coherence in twisted bilayer graphene”. In: *Phys. Rev. B* 81 (16 2010), p. 161405.
- [23] P. Moon and M. Koshino. “Optical absorption in twisted bilayer graphene”. In: *Phys. Rev. B* 87 (20 2013), p. 205404.
- [24] N. N. T. Nam and M. Koshino. “Lattice relaxation and energy band modulation in twisted bilayer graphene”. In: *Phys. Rev. B* 96 (7 2017), p. 075311.
- [25] H. C. Po et al. “Origin of Mott Insulating Behavior and Superconductivity in Twisted Bilayer Graphene”. In: *Phys. Rev. X* 8 (3 2018), p. 031089.
- [26] J. M. B. Lopes dos Santos, N. M. R. Peres, and A. H. Castro Neto. “Continuum model of the twisted graphene bilayer”. In: *Phys. Rev. B* 86 (15 2012), p. 155449.
- [27] G. Tarnopolsky, A. J. Kruchkov, and A. Vishwanath. “Origin of Magic Angles in Twisted Bilayer Graphene”. In: *Physical Review Letters* 122.10 (2019).
- [28] G. A. Tritsarlis et al. “Perturbation theory for weakly coupled two-dimensional layers”. In: *Journal of Materials Research* 31.7 (2016), pp. 959–966.
- [29] A. Watson, T. Kong, and M. Luskin. “Bistritzer-MacDonald dynamics of wave-packets in twisted bilayer graphene”.
- [30] A. B. Watson and M. Luskin. “Existence of the first magic angle for the chiral model of bilayer graphene”. In: *Journal of Mathematical Physics* 62.9 (2021), p. 091502.